East-west variabilities of N2 fixation activity in the subtropical North Pacific Ocean in summer: the field evidence of iron and phosphorus co-limitation in the western area

East-west variabilities of N_2 fixation activity in the subtropical North Pacific Ocean in summer: potential field evidence of the phosphorus and iron co-limitation in the western area

S. Horii[1,2*], K. Takahashi[2], T. Shiozaki[3], S. Takeda[4], M. Sato[2,4], T. Yamaguchi[2,5], S. Takino[2], F. Hashihama[6], Y. Kondo[4], T. Takemura[7], and K. Furuya[8]

[1] Fisheries Resources Institute, Japan Fisheries Research and Education Agency, 1551-8, Taira-machi, Nagasaki-shi, Nagasaki, 851-2213, Japan

[2] Department of Aquatic Bioscience, Graduate School of Agricultural and Life Sciences, The University of Tokyo, 1-1-1 Yayoi, Bunkyo-ku, Tokyo, 113-8657, Japan

[3] Atmosphere and Ocean Research Institute, The University of Tokyo, 5-1-5 Kashiwanoha, Kashiwa-shi, Chiba, 277-0882, Japan

[4] Graduate School of Fisheries and Environmental Sciences, Nagasaki University, 1-14 Bunkyo-machi Nagasaki-shi, Nagasaki, 852-8521, Japan

[5] Fisheries Resources Institute, Japan Fisheries Research and Education Agency, 2-12-4 Fukuura, Yokohama-shi, Kanagawa, 236-8648, Japan

[6] Department of Ocean Sciences, Tokyo University of Marine Science and Technology, 5-7 Konan, Minato-ku, Tokyo, 108-8477, Japan

[7] Research Institute for Applied Mechanics, Kyushu University, 6-1 Kasugakouen, Kasuga-shi, Fukuoka, 816-8580, Japan

[8] Institute of Plankton Eco-engineering, Soka University, 1-236 Tangi, Hachiohji-shi, Tokyo, 192-8577, Japan

Corresponding author: Sachiko Horii (shorii@affrc.go.jp)

Key Points:

- Along the zonal transect in the subtropical North Pacific, N_2 fixation activity was high in the central area (150–180°W)
- The central North Pacific was characterized by intermediate iron and phosphorus supply in the euphotic zone
- East-west gradient of phosphorus availability controls the N_2 fixation in the North Pacific through likely co-limitation with iron

Abstract

In the subtropical North Pacific, the east-west gradient of iron deposition as atmospheric Asian dust strongly affects the zonal distribution of biological N_2 fixation activity in numerical models, but the in-situ relationship at a basin-scale is not well examined. We examined the trans-Pacific zonal variation in N_2 fixation activity on 23°N in summer along with environmental parameters that potentially influence diazotrophy. Dissolved inorganic iron (DFe) was consistently low (<0.4 nM) throughout the transect. The atmospheric dust iron (dust-Fe) flux increased westward, whereas phosphate and labile phosphoric monoesters in the surface decreased westward. N_2 fixation varied between 34.6–298 μmol-N m^{-2} d^{-1} and was high (>200 μmol-N m^{-2} d^{-1}) in the central area (150–180°W). N_2 fixation rates significantly increased with dust-Fe input only in the western area (137–180°E), whereas the contribution of DFe diffused from below the euphotic zone was often larger in the eastern area (120–170°W). N_2 fixation was considerably low in the phosphate-depleted western area despite the excess amount of iron relative to phosphate, and it increased with the labile phosphoric monoesters stock. These indicated that N_2 fixation was primarily limited by phosphorus in the western area, though this activity also increased with iron supply from dust, likely due to phosphorus-iron co-limitation. In contrast, in the phosphorus-repleted eastern area, iron supplied from dust and below the euphotic zone appeared to limit N_2 fixation. Overall, N_2 fixation in the subtropical North Pacific was likely limited by zonally different factors relating to iron and phosphorus availability.

Plain Language Summary

N_2 fixation, a process that converts N_2 gas into ammonia, substantially affects biological production in subtropical ecosystems, where nitrogenous nutrients are scarce. The availability of both iron and phosphorus are primary factors controlling the growth of N_2-fixing organisms. In North Pacific subtropical waters, iron input as atmospheric Asian dust is considered to control the east-west variation in N_2 fixation; however, their relationship is not well-examined. Here, we investigated the trans-Pacific distribution of N_2 fixation activity with iron and phosphorus availability. Our results show that dust input correlates with N_2 fixation in the western area (137–180°E), which is in contrast with the eastern area (120–170°W), where vertically diffused iron was also important. In the phosphate-depleted western area, N_2 fixation positively correlated with the proxies of phosphorus supply, suggesting phosphorus limitation. This indicates phosphorus availability substantially controls the zonal distribution of N_2 fixation in the subtropical North Pacific through co-limitation with iron. The limitations are relaxed in the central area (150–180°W), likely due to elevated nutrient supply caused by bottom topography, resulting in a peak in N_2 fixation. Therefore, the dynamics of both iron and phosphorus must be considered simultaneously to predict the response of N_2 fixation to environmental changes.

1 Introduction

Biological dinitrogen (N_2) fixation, which is the process of converting N_2 gas into ammonia by specialized prokaryotes called diazotrophs, is a major new nitrogen source in the global oceans (Falkowski et al., 1998; Galloway et al., 2004). This process is particularly important for new production in oligotrophic subtropical regions. The subtropical ocean occupies 40% of the global oceans, and thus factors controlling the N_2 fixation activity are critical to understanding the global biogeochemical cycles (Karl et al., 2002).

In addition to temperature (Carpenter, 1991), the growth of diazotrophs in the subtropical ocean is largely affected by the availability of essential nutrients, especially iron and phosphorus, as it is not limited by nitrogen availability as in the case of other marine phytoplankton (Sohm et al., 2011b; Ward et al., 2013). Among these, iron input from atmospheric dust deposition is considered a primary factor controlling the basin-scale distribution of diazotrophs (Dutkiewicz et al., 2012; Moore et al., 2009; Ward et al., 2013) due to the substantial iron requirement for nitrogenase enzyme activity (Berman-Frank et al., 2001). Additionally, the availability of phosphorus, which plays an essential role in cell growth and energy supply for diazotrophs, is also important for controlling N_2 fixation (Sohm et al., 2011b; Ward et al., 2013), as suggested by nutrient addition experiments (Grabowski et al., 2008; Tanita et al., 2021; Watkins-Brandt et al. 2011; Wen et al., 2022).

The subtropical North Pacific has an east-west gradient of iron input from atmospheric dust deposition and phosphorus stock; atmospheric dust deposition flux from the Asian continent decreases eastward (Duce & Tindale, 1991), while both phosphate and dissolved organic phosphorus (DOP) concentrations decrease westward (Hashihama et al., 2009; 2020; Yamaguchi et al., 2021). However, N_2 fixation in the subtropical North Pacific is generally considered iron-limited rather than phosphorus-limited because of the vastness of the basin (Sohm et al., 2011b; Wang et al., 2019), which restricts iron supply from the Asian continent, and the supply of excess phosphorus relative to the Redfieldian phytoplankton demands in the eastern region (Deutsch et al. 2007). Therefore, prognostic biogeochemical models generally predict the westward increase in N_2 fixation at a basin-scale in the subtropical North Pacific Ocean with an increase in dust deposition (Dutkiewicz et al., 2012; Monteiro et al., 2011; Wang et al., 2019). However, in-situ measurements of N_2 fixation activity in the western subtropical North Pacific in previous studies (39–573 μmol N m^{-2} d^{-1}; Shiozaki et al., 2009, 2010; Tanita et al., 2021; Wen et al., 2022) are not necessarily higher than those in the central and eastern regions, which show rates between 87 and 520 μmol N m^{-2} d^{-1} (Montoya et al., 2004; Wilson et al., 2008; Böttjer et al., 2017; Shiozaki et al., 2017). This inconsistency suggests that iron input through atmospheric dust deposition is not the single factor controlling the geographic variation of N_2 fixation activity in the subtropical North Pacific, although no adequate observation to examine this has been made to date.

Here, we conducted a trans-Pacific observation at 23°N from 120°W to 137°E in summer (August–September) to examine the east-west variations in N_2 fixation in relation to iron and phosphorus availability. As a proxy for iron supply, the iron flux from atmospheric dust deposition (dust-Fe) was simulated during cruise periods, and the concentration of dissolved inorganic iron (DFe) in the vertical profile was measured. We examined the concentrations of the labile fraction of phosphoric monoesters in addition to phosphate using a highly sensitive analytical method. Phosphoric esters comprise the majority (80–85%) of the DOP pool in various oceanic regions (Young & Ingall, 2010). Labile phosphoric monoesters are a necessary phosphorus source as phosphoric monoesterase activity increases under low phosphate

conditions in the Atlantic and Pacific oceans (Mahaffey et al., 2004; Yamaguchi et al., 2019, 2021). Additionally, the abundance of *nifH* genes of major diazotrophs was determined to examine their relationship with the geographical variation in N_2 fixation activity. This study shows the importance of phosphorus as a controlling factor affecting the distribution of N_2 fixation in the subtropical North Pacific Ocean, as well as iron.

2 Materials and Methods

2.1 Study site, physical and chemical parameters, and chlorophyll *a*

This study was conducted at 12 stations from 21 August to 1 October 2017, along the zonal transect from 120°W to 137°E on the 23°N line in the North Pacific subtropical region by the KH-17-4 cruise onboard the R/V *Hakuho-maru* (Figure 1 and Table 1). Temperature and salinity profiles were obtained using a conductivity, temperature, and depth (CTD) system (Sea-Bird Electronics Inc., Bellevue, WA, USA), and light intensity was measured using a Hyper Profiler (Satlantic LP, Halifax, NS, Canada). Euphotic zone depth was defined as 1% light depth. The mixed layer depth was defined as where the temperature was 0.2°C less than that at a depth of 10 m (de Boyer Montégut et al., 2004).

All water samples were collected using an acid-cleaned bucket or Teflon-coated 12-L Niskin-X bottles on a CTD-Carousel system connected to a Vectran cable between the surface and a depth of 200 m. The water samples for the macro-nutrients and chlorophyll *a* (chl *a*) were directly collected from Niskin-X bottles or buckets into plastic bottles. The concentrations of nitrate and phosphate were determined onboard using a super-sensitive colorimetric system (Hashihama et al., 2009). The detection limits of both nitrate and phosphate were 3.0 nM. When the concentration was higher than 1 μM, the samples were frozen, and the concentrations were determined using an AACSII auto-analyzer on land (Bran+Luebbe, Hamburg, Germany). The concentration of labile phosphoric monoesters was measured using the enzymatic hydrolysis method described by Yamaguchi et al. (2021), and the detection limit was 3.4 nM. For chl *a*, an aliquot of 260 mL water was gently filtered using 25-mm Whatman GF/F filters (GE HealthCare, IL, USA), and the concentration was fluorometrically measured using a 10-AU fluorometer (Turner Designs, CA, USA) after extraction with *N, N*-dimethylformamide (Suzuki & Ishimaru, 1990; Welschmeyer, 1994).

Table 1. Summary of N_2 fixation activity and environmental variables at each station during the KH-17-4 cruise.

Station	Date (GMT)	Latitude	Longitude	1% light depth [m]	SST [°C]	Dust-Fe [nmol m^{-2} day^{-1}]	DFe [µmol m^{-2}]	Phosphate [mmol m^{-2}]	Phosphoric monoesters [mmol m^{-2}]	N_2 fixation activity [µmol N m^{-2} d^{-1}]	Primary production [mmol C m^{-2} day^{-1}]	N_2 fix/PP ratio [%]
1	21 August 2017	23° 00' N	120° 00' W	104	24.6	65.7	32	22	2.9	75.5	14.2	3.5
2	25 August 2017	23° 00' N	130° 00' W	116	23.9	79.2	39	18	2.5	157	24.3	4.3
3	28 August 2017	23° 00' N	140° 00' W	110	24.7	125	33	8.2	2.4	129	15.4	5.5
4	31 August 2017	23° 00' N	150° 00' W	106	25.9	136	51	5.3	2.0	283	25.1	7.4
5	3 September 2017	21° 30' N	160° 00' W	104	27.6	156	39	8.6	1.9	298	19.8	9.9
6	14 September 2017	21° 30' N	170° 00' W	108	28.7	278	46	2.5	1.9	239	19.4	8.1
7	17 September 2017	23° 00' N	180° 00' W	111	28.3	667	11	3.1	1.9	239	17.2	9.2
8	20 September 2017	23° 00' N	170° 00' E	113	28.3	667	38	1.9	1.3	127	14.0	6.0
9	23 September 2017	23° 00' N	160° 00' E	114	29.3	533	46	0.58	1.2	96.2	11.7	5.4
10	27 September 2017	23° 00' N	150° 00' E	103	29.1	400	43	0.77	0.14	44.3	24.7	1.2
11	30 September 2017	23° 00' N	140° 00' E	106	29.8	194	56	2.2	0.36	34.6	13.3	1.7
12	1 October 2017	23° 00' N	137° 00 E	117	29.9	321	31	0.51	1.1	67.9	21.6	2.1

Notes: SST indicates sea surface temperature. Dust-Fe indicates 14-days average of daily iron input as atmospheric dust deposition modeled by SPRINTARS before the observation. The integrated amounts of dissolved inorganic iron (DFe), phosphate and labile phosphoric monoesters in the euphotic zone were shown. The euphotic zone depth was defined as the depth of 1% light depth, but it was substituted by the depth of subsurface chlorophyll maximum (102–140 m) for DFe

amount. The integrated rates in the water column were shown for N_2 fixation activity. N_2 fix/PP ratio indicates N_2 fixation activity × 6.6/primary production × 100, 6.6 is the Redfield ratio.

Samples for dissolved inorganic iron (DFe) concentration were taken from trace-metal clean Niskin-X bottles, which were placed in a clean air booth immediately after recovery, based on GEOTRACES methods. Seawater was typically taken from depths of 10, 20, 50, 100, 150, 200 and 400 m and the subsurface chl *a* maximum (SCM), and filtered through an AcroPak 200 Capsule filter unit having 0.2 μm pore-size Supor Membrane (Pall Co., NY, USA) attached directly to the spigot with silicon tubing under pressure by compressed clean air. Filtered seawater samples were collected in acid-cleaned 125-mL low-density polyethylene (LDPE) bottles and acidified to pH <1.7 with 20% quartz-distilled HCl (TAMAPURE AA-100, Tama Chemicals Co., Kanagawa, Japan). The acidified water samples were stored at room temperature for more than one year before analysis. The concentration of DFe was determined by cathodic stripping voltammetry after complexation of 2, 3-dihydroxynaphthalene with ferric ions and the standard addition method, as described by Obata and van den Berg (2001). The detection limit of the DFe was 0.03 nM.

In nitrogen-depleted water, the growth rate of diazotrophs is substantially controlled by the balance of availability between phosphorus and iron (Ward et al., 2013; Garcia et al., 2015). Thus, relative magnitude of decoupling between iron and phosphate amount, i.e., DFe*, in the euphotic zone was calculated as DFe (μmol m^{-2}) − phosphate (μmol m^{-2}) × 0.48/1000 based on previous studies (Nishioka & Obata, 2017; Rijkenberg et al., 2018). The value of 0.48 mmol mol^{-1} used in the equation represents the median of the ratio of DFe to phosphate in the water mass at 400 m depth during the cruise.

2.2 N_2 fixation activity and primary production

N_2 fixation activity and primary production were measured based on the ^{15}N-^{13}C dual inlet technique, which combined the $^{15}N_2$ gas dissolution method (Mohr et al., 2010) with a ^{13}C primary production assay (Hama et al., 1983), for the six depths corresponding to incident light levels of 100%, 25%, 10%, 1%, and 0.1%, and at a depth of 10 m. Water samples for incubation were collected in duplicate acid-cleaned 4.5 L polycarbonate bottles covered by neutral-density screens to adjust the light levels with initial samples, which were immediately filtered onto pre-combusted GF/F filters. For incubation, $^{15}N_2$-enriched seawater was prepared at each station. We degassed the surface water by applying a vacuum using a Sterapore membrane unit (20M1500A; Mitsubishi Rayon Co. Ltd., Tokyo, Japan) and then injected 10 mL of $^{15}N_2$ gas (99% atom% ^{15}N; SI Science, Saitama, Japan) per 1 L of media. After the $^{15}N_2$ gas was dissolved completely, 111 mL of $^{15}N_2$-enriched seawater and ^{13}C-labeled sodium bicarbonate (CLM-441, 99% atom% ^{13}C; Cambridge Isotope Laboratories Inc., MA, USA) were added. The final tracer concentration of ^{13}C was 200 μM. Although the volume of dissolved N_2 was calculated using the equation given by Weiss (1970), this calculation may underestimate the rates by approximately 20% (White et al., 2020). Commercial $^{15}N_2$ gas could be contaminated by ^{15}N-labeled nitrate and ammonium (Dabundo et al., 2014); however, the contamination of the SI Science $^{15}N_2$ gas was negligible (Shiozaki et al., 2015). Seawater was incubated on the deck in a running seawater bath for 24 h and then filtered onto pre-combusted GF/F filters. All filter samples were kept at −20°C until later measurements on land. For the measurement, the filter samples were oven-dried at 50°C, exposed to HCl fumes for 2 h to remove the carbonate, and dried again at 50°C. The nitrogen and carbon contents and their stable isotopic ratios were determined using a DELTA V Advantage mass spectrometer (Thermo Electron, MA, USA) connected to an elemental analyzer. We used five different working standards of amino acids provided by Shoko Science Co. Ltd. (Kanagawa, Japan) with different isotope ratios, from −7.6 to 20.6‰ for $\delta^{15}N$ and from −32.3 to −10.7‰ for

198 $\delta^{13}C$ to obtain the calibration curves; moreover, a working standard with the $\delta^{15}N$ of −1.2‰ and
199 $\delta^{13}C$ of −19.9‰ was measured every 10 samples to correct the baselines (Sato & Suzuki 2010).
200 The rates of N_2 fixation and primary production were calculated according to Montoya et al.
201 (1996) and Hama et al. (1983), respectively. We considered N_2 fixation activity to be significant
202 when the proportion of ^{15}N in the nitrogen content for each incubated bottle was higher than that
203 of the initial sample by 0.00146 atom% (Montoya et al., 1996). The in-situ concentration of
204 dissolved inorganic carbon was set to 2 mM for all batches for the calculation of primary
205 production (Christian et al., 1997).

206 2.3 DNA analyses for determining diazotroph distribution

207 Water samples for qPCR analyses of *nifH* genes of major diazotrophs were collected in
208 1.1 L polypropylene bottles from the same Niskin bottles concurrently with the sampling for
209 determining N_2 fixation activity and were filtered onto 0.2 μm Nuclepore filters (GE HealthCare,
210 IL, USA). All filter samples were kept frozen at −20°C until analysis. DNA was extracted using
211 a ChargeSwitch Forensic DNA Purification Kit (Invitrogen, Carlsbad, CA, USA), following the
212 manufacturer's instructions. We quantified six groups of diazotrophs known to be significant in
213 the North Pacific subtropical water (Shiozaki et al., 2017); heterotrophic γ-proteobacterium γ-
214 24774A11, symbiotic cyanobacteria UCYN-A1 associated with haptophytes, *Richelia*
215 *intracellularis* associated with diatoms belonging to *Rhizosolenia clevei* (RR), *R. intracellularis*
216 associated with diatoms belonging to *Hemiaulus hauckii* (RH), filamentous cyanobacteria
217 *Trichodesmium* spp., and unicellular cyanobacterium *Crocosphaera watsonii*. The sets of
218 primers, probes, and standards are described in Supporting Information Table S1. We conducted
219 a qPCR assay using the Mini Opticon Real-Time PCR System (BIO-RAD, CA, USA). The 20
220 μL reactions contain10 μL 2×PreMix Ex Taq (Probe qPCR, Takara Bio Inc., Shiga, Japan), 6.4
221 μL Milli-Q water, 2 μL template DNA, 0.6 μL for each of the10 μM forward and reverse
222 primers, and 0.4 μL for 10 μM Taqman probe. At least triplicate PCR amplifications were
223 performed for each sample with the following parameters: 95°C for 5 min, followed by 49 cycles
224 of 95°C for 4 s and 60°C for 11 s. Standards consisting of six 10-fold dilutions of *nifH* gene
225 fragments (10^6–10^1 copies) and a negative control were prepared for each plate. The copy
226 numbers of the target genes in the DNA samples were calculated from the mean Ct value for
227 each sample. The r^2 values of the standard curves were always >0.99, and no signal was detected
228 in the negative controls. PCR efficiencies were between 89.0% and 111.1%, and the detection
229 limit was 75 copies/L. The coefficient of variation (CV) of replicate samples were generally
230 <60%, but increased up to 180% when the concentration was <1000 copies/L.

231 2.4 Atmospheric dust deposition

232 Daily dry and wet deposition of soil dust was calculated using a three-dimensional
233 aerosol climate model SPRINTARS version 6.1.0 at 1.12° × 1.12° resolution, which was
234 developed using the framework of atmospheric general circulation model MIROC and verified
235 for the dust transport in the North Pacific (Takemura et al., 2000, 2002, 2005). We assumed that
236 the iron content of dust was 3.5%, which is the average value of the Earth's crust, (Duce &
237 Tindale 1991) and calculated the daily flux of iron as atmospheric dust (dust-Fe) at each station.
238 The 14-day average of daily deposition before the date of observation was used for the analyses,
239 according to Hashihama et al. (2009).

240 2.5 Supply of iron and phosphate to the euphotic zone

241 To estimate the relative supply of iron from different sources to the euphotic zone, the
242 fluxes of soluble iron leached from dust-Fe and of DFe vertically diffused from below the
243 euphotic zone were calculated. The iron solubility of dust-Fe was set as 0.45%, a common value
244 used in model studies to estimate atmospheric iron input to the ocean on a basin scale (Luo et al.,
245 2008; Adebiyi et al., 2023). The vertical DFe diffusion flux was calculated using the equation;
246 Flux = Kz × d[DFe]/dz, in which Kz is eddy diffusivity. The vertical gradient of DFe, d[DFe]/dz,
247 was calculated using the DFe concentrations at SCM and 200 m depth. Further, we used the eddy
248 diffusivities observed during the same cruise in the subsurface pycnocline (Itoh et al., 2021).
249 Total Fe flux was calculated by adding soluble dust-Fe flux and vertical DFe diffusion flux. In
250 addition, vertical phosphate diffusion flux from below the euphotic zone was calculated in a
251 similar manner using phosphate concentration at 1% light depth and 200 m depth. The relative
252 magnitude of decoupling between iron and phosphate supply (total Fe* flux) was calculated
253 based on the concept of DFe* (the excess DFe amount relative to phosphate) using the following
254 equation: total Fe* flux = total Fe flux − vertical phosphate diffusion flux × 0.48/1000 (Nishioka
255 & Obata, 2017; Rijkenberg et al., 2018). The value 0.48 mmol mol^{-1} in the equation represents
256 the median of the ratio of DFe to phosphate in the water mass at 400 m depth during the cruise.

257 **3 Results**

258 3.1 Environmental conditions

259 Sea surface temperature (SST) and sea surface salinity tended to increase westward from
260 24°C to 30°C and from 34.4 to 35.2, respectively, along the transect (Figures 2a, b). The
261 euphotic zone depth varied in the range of 104–117 m and did not show notable zonal variation
262 (Table1, Figure 2). The mixed layer depth varied from 15 to 52 m and was deepest around the
263 stations in the center of the transect (St. 4 and 5), while those in other stations were relatively
264 constant (mostly 20–40 m). The concentration of chl *a* at the surface did not show an apparent
265 east-west variation. However, SCM was always observed around the 1% light depth, with the
266 concentration being relatively high (>0.3 μg/L) at the westernmost three stations (St. 10–12) in
267 addition to St. 4–5, in which the mixed layer depth was relatively deep (Figure 2c). Nitrate was
268 mostly depleted (<10 nM) in the euphotic zone (Figure 2d) and there was no clear zonal gradient.
269 Phosphate and labile phosphoric monoesters in the euphotic zone decreased westward from >200
270 nM to <10 nM and from >30 nM to <10 nM, respectively (Figures 2e and f). The depth-
271 integrated amount of phosphate and phosphoric monoesters in the euphotic zone decreased
272 westward from 25 to <2.5 mmol m^{-2} with an increasing proportion of phosphoric monoesters
273 (Figure 3a, Table 1). Neither the DFe concentration at a depth of 10 m (0.11–0.40 nM, data not
274 shown) nor the euphotic-zone integrated amount (11–56 μmol m^{-2}) varied across the zonal
275 transect (Figure 3b, Table 1). In contrast, the modeled atmospheric dust-Fe flux generally
276 increased westward (Figure 3c, Table 1). The mean value of dust-Fe flux in the area west of 180°
277 (423 ± 184 nmol Fe m^{-2} day^{-1}; St. 7–12) was significantly higher than that in the area east of
278 180° (154 ± 74.4 nmol Fe m^{-2} day^{-1}; St. 1–6) (p <0.05, t-test).

279 3.2 N_2 fixation activity and primary production

280 The rates of N_2 fixation activity and primary production were the highest in the upper
281 layer, from the surface to a depth of 20–30 m, which corresponded to the upper layer at 25%
282 light depth (Figures 2g and f). The rates between 0.1 and 1% light depth were often below the

detection limits; hence, we considered them zero. The maximum and depth-integrated N_2 fixation in the water column varied between 0.5–7.1 nmol N L^{-1} day^{-1} and 34.6–298 μmol N m^{-2} day^{-1}, respectively, and increased in the central region from St. 4 to 7 (Figures 2g and 3c, Table 1). Although no significant correlation was found between integrated N_2 fixation and any of the environmental variables throughout the transect (p >0.05; Figure 4, Supporting Information Figure S3), both iron and phosphorus showed significant correlations (p <0.05) with N_2 fixation depending on the zonal range: east (St. 1–6) and west (St. 7–12) of 180°. In the western area, N_2 fixation activity was significantly and positively correlated with dust-Fe flux and negatively correlated with euphotic-zone DFe amount (p <0.05, Figures 4a and b). In contrast, no significant correlation was observed between N_2 fixation activity and dust-Fe flux or the DFe amount in the eastern area (Figures 4a and b). Although N_2 fixation activity did not show a significant relationship with phosphate stock in both areas, N_2 fixation showed significant positive and negative correlations with a stock of phosphoric monoesters in the western and eastern regions, respectively (p <0.05, Figures 4c and d). Depth-integrated amount of total DOP (Yamaguchi et al. 2021) did not show a significant relationship with N_2 fixation activity (p >0.05, data not shown).

Compared with N_2 fixation, the zonal variation in the depth-integrated primary production was relatively small, which ranged between 11.7–25.1 mmol C m^{-2} day^{-1} (Table 1, Supporting Information Figure S5a). Generally, the primary production was positively correlated with depth-integrated N_2 fixation, except at the western end of the transect from St. 10 to 12 (p <0.05, Supporting Information Figure S5b). The calculated contribution of the fixed nitrogen to primary production was the highest in the central region (7.4–9.9%; St. 4–7) and consistently lower at the western end of the transect (1.2–2.1%; St. 10–12) than those at other stations (Supporting Information Figure S5a).

3.3 Iron and phosphate fluxes into the euphotic zone

The regional patterns of the calculated iron fluxes differed between the soluble dust-Fe and vertical DFe diffusion (Figure 5a). The soluble dust-Fe flux was higher in the western area (0.87–3.1 nmol Fe m^{-2} day^{-1}, St. 7–12) than in the eastern area (0.30–1.3 nmol Fe m^{-2} day^{-1}, St. 1–6), while the vertical DFe diffusion flux largely decreased westward from 3.1 nmol Fe m^{-2} day^{-1} to the negative values (Figure 5a). The contribution of soluble dust-Fe to the total Fe flux (soluble dust-Fe flux + vertical DFe flux) was consistently high (89–100%) in the western area, while the contribution of vertically diffused DFe increased to 40–91% in the eastern area, except at St. 3 (Figure 5a).

Vertical phosphate diffusion flux also exhibited east-west variation. It was higher at easternmost St. 1 and 2 (4.7–9.5 μmol P m^{-2} day^{-1}), whereas it was considerably lower at westernmost St. 11 and 12 (0.1–0.3 μmol P m^{-2} day^{-1}; Figure 5b). Intermediate fluxes, ranging from 0.6 to 1.9 μmol P m^{-2} day^{-1}, were observed from St. 3 to St.10 (Figure 5b). Overall, phosphate flux in the eastern area (St. 1–6) was higher than those at the stations in the western area except at St. 10.

Total Fe* flux (magnitude of excess iron supply relative to phosphate) was relatively high (0.4–3.1 nmol m^{-2} day^{-1}) in the central region from St. 4–9 as well as St. 12, whereas lower total Fe* fluxes, ranging from –1.1 to 0.2 nmol m^{-2} day^{-1}, were observed at stations in the eastern (St. 1–3) and western (St. 10–11) areas (Figure 5c). Euphotic-zone DFe* (excess DFe amount relative to phosphate in the euphotic zone) increased westward from St. 1–3 (21–30 μmol m^{-2}) to St. 4–6 (35–48 μmol m^{-2}) in the eastern area (Figure 5c). In the western area,

328 euphotic-zone DFe* showed the lowest value (9.5 μmol m^{-2}) at St. 7, whereas it increased
329 westward to 55 μmol m^{-2} at St. 11, with the westernmost St. 12 showing an intermediate value
330 (31 μmol m^{-2}).
331 Total Fe* flux was significantly and positively related to the N_2 fixation activity both in
332 the eastern and western areas (p <0.05, Figure 6a). Euphotic-zone DFe* was also significantly
333 and positively correlated to the N_2 fixation activity in the eastern area, whereas it showed a
334 significant negative correlation with the N_2 fixation activity in the western area (p <0.05, Figure
335 6b).

336 3.4 Distributions of major diazotrophs

337 The *nifH* genes quantified in this study were mainly composed of three cyanobacteria,
338 *Crocosphaera watsonii*, *Trichodesmium* spp., and UCYN-A1, whose depth-integrated
339 abundances were more than ten times higher than those of the other diazotrophs, namely γ-
340 24774A11, and two types of *Richelia intracellularis* (Figure 7 and Supporting Information S6).
341 *C. watsonii* and *Trichodesmium* spp. were widely distributed between St. 4 and St. 12 with the
342 maximum abundances of 10^5 and 10^4 copies/L, respectively, whereas they rarely occurred at St.
343 1–3 (Figure 7, Supporting Information Figures S6a and b). Contrastingly, UCYN-A1 dominated
344 the quantified community at the eastern stations from St. 1 to 3 at a concentration of up to 10^5
345 copies/L (Figure 7, Supporting Information Figure S6c). The total abundance of the diazotrophs
346 was especially high at St. 4 and 5, corresponding to the stations where high N_2 fixation was
347 found (Figure 7). At these stations, the distribution ranges of *C. watsonii*, and *Trichodesmium*
348 spp. with high concentration (>10^4 copies/L) extended deeper than 50 m (Supporting Information
349 Figures S6a and b).

350 **4 Discussion**

351 4.1 Factors determining the zonal distribution of N_2 fixation in this study

352 The trans-Pacific observation along the 23°N transect revealed that the N_2 fixation
353 activity was particularly high (238–283 μmol N m^{-2} day^{-1}) in the central area from 180° to
354 150°W, and decreased both eastward and westward (34.6–157 μmol N m^{-2} day^{-1}). This
355 geographical variation in N_2 fixation is different from the annually averaged pattern simulated by
356 numerical models, which increased westward, reflecting the westward increase in the Asian dust
357 input (Dutkiewicz et al., 2012; Monteiro et al., 2011). This difference may be expected due to
358 seasonal variations in dust deposition flux; however, the westward increasing pattern of the dust
359 input in the North Pacific during the cruise was similar to those in the model simulations (Figure
360 3b). Therefore, our results suggest that the basin-scale distribution of N_2 fixation activity in the
361 subtropical North Pacific is substantially controlled not only by dust-Fe input but also by other
362 factors.
363 The SST observed along the transect ranged from 24 to 30°C, suggesting that the
364 temperature was not an important factor in controlling the N_2 fixation activity since the observed
365 SST range was within the optimum temperatures of dominant diazotrophic cyanobacteria (20–
366 26°C for UCYN-A1; >25°C for *Crocosphaera watsonii* and *Trichodesmium* spp.; Tang & Cassar
367 2019). In this study, nitrate was consistently depleted in the euphotic zone, while the daily-
368 integrated light intensity did not correlate with N_2 fixation activity (p >0.05, Supporting
369 Information Figure S1). Therefore, it is more likely that substantial supply of nutrients such as
370 iron and phosphate was essential to affect the zonal variation of N_2 fixation activity.

In this study, the DFe concentration at a depth of 10 m was substantially low (0.11–0.40 nM) and within the range of those when iron limitation on diazotrophs occurred in subtropical open waters (Cerdan-Garcia et al., 2022; Tanita et al., 2021), indicating that bio-available iron was scarce throughout the study area. Therefore, iron input, rather than stock, is a more appropriate parameter to examine the relationship between iron availability and N_2 fixation. The rates of N_2 fixation positively correlated to the dust-Fe input in the western area (St. 7–12), where total Fe flux was primarily composed of dust-Fe; no significant correlation was observed in the eastern area (St. 1–6), where dust-Fe input was lower than that in the western area. However, the highest rates of N_2 fixation in the eastern area were similar to those in the western area (238–283 μmol N m^{-2} day^{-1}; Table 1), likely owing to the contribution of vertically diffused DFe from below the euphotic zone, accounting for > ca. 40% of the total Fe flux (Figure 5a). These results suggest that, in addition to dust-Fe, the iron supply from layers deeper than the euphotic zone was important for controlling N_2 fixation activity in the eastern area. Itoh et al. (2021) reported the enhancement of vertical mixing at St. 4–6 (150–170°W), where the highest N_2 fixation was observed, due to the effect of Mid-Pacific Seamounts and Hawaiian Ridge. Furthermore, N_2 fixation activity in the eastern area correlated significantly with the eddy kinetic energy, which also supports the importance of vertically supplied DFe (Supporting Information Figure S3e). In contrast to DFe, the phosphate concentration showed an apparent east-west gradation. In the western area, phosphate in the euphotic zone was depleted to <50 nM, which corresponded to the level capable of limiting N_2 fixation activity in the North Pacific (Letelier et al., 2019; Tanita et al., 2020; Wen et al., 2022). Conversely, phosphate was repleted (>50 nM) in the eastern area.

We found that N_2 fixation activity correlated positively with total Fe* flux (excess iron supply relative to phosphate) in both the eastern and western areas (p <0.05, Figure 6a), although the correlation with total Fe flux was significant only in the western area (p <0.05; Supporting information Figure S4b). These observations indicate that in the subtropical North Pacific, the iron supply relative to phosphate affects the N_2 fixation, as has been previously suggested (Garcia et al., 2015; Ward et al., 2013). Correspondingly, a positive correlation between N_2 fixation activity and euphotic-zone DFe*, which reflects the residual nutrient balance, was found in the eastern area (Figure 6b), indicating that primarily iron limited the activity. In contrast, in the western area, euphotic-zone DFe* was negatively correlated to N_2 fixation, suggesting substantial suppression of the activity despite the excess iron. This negative correlation can be attributed to the magnitude of phosphate depletion among the western stations. Furthermore, the positive correlation between N_2 fixation activity and the standing stock of labile phosphoric monoesters in the western area (Figure 4b) supports the hypothesized phosphorus limitation of N_2 fixation in the western area. During the same cruise, high rates of phosphoric monoesterase activity were observed in this area (Yamaguchi et al., 2021).

Overall, the present study shows that limiting factors controlling N_2 fixation in the subtropical North Pacific differ between the eastern and western areas. In the eastern area, where phosphorus was repleted, iron, supplied from below the euphotic zone and from dust, appeared to be the primary limiting factor of N_2 fixation. In the western area, phosphorus was more likely to primarily limit the activity, although N_2 fixation also increased with iron supply, mainly from dust-Fe. This phenomenon can be explained by independent nutrient co-limitation in the western area by two elements (phosphorus and iron) that are biochemically mutually exclusive in general but are also both detected in low concentrations (Saito et al. 2008). The co-limitation of iron and phosphorus on N_2 fixation activity was reported in the phosphate-depleted waters of the Atlantic

Ocean (Mills et al., 2004) and was recently indicated through nutrient enrichment experiments in the western North Pacific Ocean (Tanita et al., 2021; Wen et al., 2022). Therefore, the results of this study are supported by an experimental approach. The co-limitation is expected to relax eastward with increasing phosphate concentration in the euphotic zone, as observed at St. 7 (180°), which showed high rates of N_2 fixation activity associated with relatively high concentrations of phosphate and phosphoric monoesters. In contrast, iron limitation in the eastern area is expected to relax around St. 4–6 (150–170°W) due to vertically supplied DFe from below the euphotic zone owing to the effect of Mid-Pacific Seamounts and Hawaiian Ridge (Itoh et al., 2021) in addition to dust-Fe input from the Asian continent. Furthermore, vertically supplied phosphate together with DFe can create favorable conditions for diazotroph growth in this area (Figures 5a and b). Overall, zonal variation of N_2 fixation activity in the subtropical North Pacific is likely controlled by different processes underlying iron and phosphorus supply, resulting in the N_2 fixation pattern observed in this study with a prominent peak between 150–180°W.

4.2 East-west variability in diazotroph distribution in relation to N_2 fixation

The maximum abundance of diazotrophs observed in this study was 10^5 copies/L for *C. watsonii* and 10^4 copies/L for *Trichodesmium* spp. and UCYN-A1. These values were consistent with those of a previous basin-scale observation for *Trichodesmium* spp. and UCYN-A1 in the subtropical gyre of the North Pacific region (<10^6 copies/L near the surface; Cheung et al., 2020). However, the composition of the quantified diazotrophs varied along the transect. UCYN-A1 dominated the quantified diazotrophs at St. 1–3, whereas *C. watsonii* and *Trichodesmium* spp. were more abundant at St. 4–12, except at St. 10 (Figure 7). This pattern was broadly consistent with the optimum temperature ranges for these diazotrophs. UCYN-A1, which was abundant in the eastern stations (St. 1–3), can occur in an environment with a relatively lower temperature range of 20–26°C in comparison with *C. watsonii* and *Trichodesmium* spp., which are abundant at temperatures exceeding 25°C (Tang & Cassar, 2019).

Abundant data are available regarding N_2 fixation at St. ALOHA (22° 45'N, 158° 00'W), which is located between St. 4 and 5, in the present study. At St. ALOHA, N_2 fixation activity is generally 100–350 μmol N m^{-2} day^{-1} and increases to 400–700 μmol N m^{-2} day^{-1} (or up to 20 nmol N L^{-1} day^{-1}) during high sea surface height (SSH) anomaly (>0.11 m; Bötjer et al., 2017). Various diazotrophs, such as *R. intracellularis* and UCYN-A1, can be dominant in summer at St. ALOHA in addition to *C. watsonii* and *Trichodesmium* spp., with an abundance of 10^9–10^{11} copies m^{-2} (Church et al., 2009). In addition, Church et al. (2009) reported that the abundance of *R. intracellularis* increased in response to a higher SSH anomaly, reaching 10^{11} copies m^{-2} and indicating its contribution to increased N_2 fixation. In the present study, however, *R. intracellularis* was less abundant (<10^8 copies m^{-2}) at St. 4 and 5, whereas that of *C. watsonii* and *Trichodesmium* spp. was 1.1–1.4 × 10^{10} copies m^{-2} in total, followed by UCYN-A1 (0.4–1.7 × 10^9 copies m^{-2}). The N_2 fixation rates (283–298 μmol N m^{-2} day^{-1} and 2–7 nmol N L^{-1} day^{-1}) were within the range of the case with a lower SSH anomaly at St. ALOHA, as the anomaly was nearly zero (–0.02 to 0.03 m) during observation in the present study (Supporting Information Figure S2b). Overall, the abundance of the major diazotrophs and the extent of N_2 fixation activity around St. 4 and 5 were similar to those at St. ALOHA, except for a less frequent occurrence of *R. intracellularis.*

Compared with that at St. 4 and 5, the abundance of the quantified diazotrophs was constantly lower at St. 6–12 (<4.0 × 10^9 copies m^{-2} or <10^5 copies/L in total). In general, *C.*

watsonii was the most abundant, followed by *Trichodesmium* spp. and UCYN-A1 (Figure 7). The depth-integrated N_2 fixation, however, exhibited an approximate 5-fold variation. Stations 6 and 7 had N_2 fixation rates (239 μmol N m^{-2} day^{-1} and 7.0 nmol N L^{-1} day^{-1} near the surface) comparable to those at St. 4 and 5, which decreased westward to St. 11 (34.6 μmol N m^{-2} day^{-1} and 0.5 nmol N L^{-1} day^{-1} near the surface). Shiozaki et al. (2017) reported similar N_2 fixation rates (116–228 μmol N m^{-2} day^{-1} and 0.8–3 nmol N L^{-1} day^{-1}) around St. 6 and 7 in summer, which agrees with our findings, but with higher abundance of cyanobacterial diazotrophs (*C. watsonii, Trichodesmium* spp. and UCYN-A1; 9.4–16.4 × 10^9 copies m^{-2} in total). Therefore, our data indicate that diazotrophs around St. 6 and 7 could achieve N_2 fixation comparable to that near the Hawaiian Islands, despite the lower abundance of the major diazotrophs, possibly because the limitation of iron and/or phosphorus was relaxed. For the stations further west (St. 8–12), a lower N_2 fixation activity with a small number of diazotrophs was observed, as previously reported (Shiozaki et al. 2010, Tanita et al. 2021), likely due to the depletion of labile phosphorus.

UCYN-A1 was exceptionally predominant in the quantified diazotrophs at St. 10 in the western area. The isotherm depths of 22–24°C were shallower at St. 10 as well (Figure 2a), probably related to high eddy diffusivity (0.85 × 10^{-5} m^2 s^{-1}) attributed to active vertical mixing due to the Marcus-Wake Seamounts (Itoh et al., 2021). Thus, UCYN-A1 could be a major diazotroph in the western area, depending on physical condition, as it increased in response to vertical mixing by eddies (Cheung et al., 2020). UCYN-A1 was also predominant in the quantified diazotrophs at easternmost St. 1–3 (0.6–3.4 × 10^9 copies m^{-2} or 10^4–10^5 copies/L), corresponding to the lower temperature. However, this abundance and the extent of N_2 fixation activity between St. 1–3 were consistently lower compared to the results of previous studies. Cheung et al. (2020) reported UCYN-A1 abundance at 10^6 copies/L in the neighboring areas (30°–40°N, 120–150°W) and Montoya et al. (2004) reported N_2 fixation activity at 10–30 nmol N L^{-1} day^{-1} (or 520 ± 160 μmol N m^{-2} day^{-1}) with an emphasis on the importance of UCYN-A. This difference may be due to the intensity of wind-driven upwelling, which controls the supply of iron and phosphate to the euphotic zone, and is positively correlated with the abundance of UCYN-A1 (Cheung et al., 2020). Another possibility is the effect of top-down controls, which have been suggested as important factors controlling diazotroph abundance (Dugenne et al., 2020; Wang & Luo, 2022). Several studies have indicated that diazotrophs are utilized by various micro- and mesozooplankton (Conroy et al., 2017; Dugenne et al., 2020).

4.3 Possible spatiotemporal variation in N_2 fixation in the subtropical North Pacific

The widespread depletion of phosphate in the euphotic zone was reported in the western part of the subtropical North Pacific, which was largely attributed to the active N_2 fixation enhanced by the abundant dust-Fe input from the Asian continent (Deutsch et al., 2001; Hashihama et al., 2009; Martiny et al., 2019). Therefore, the co-limitation of phosphorus and iron indicated in this study seems to be applicable to N_2 fixation in the western area of the subtropical North Pacific. However, the eastern limit for this co-limitation would vary on a decadal time scale with the Pacific Decadal Oscillation, which may affect the ecosystem near the Hawaiian Islands to oscillate between iron and phosphorus limitation (Letelier et al., 2019).

DOP is considered an important phosphorus source for diazotrophs in phosphate-depleted waters (Cerdan-Garcia et al., 2022; Watkins-Brandt et al., 2011). Microbes, including diazotrophs, require additional iron to utilize DOP under phosphate-depleted conditions (Browning et al., 2017; Liang et al., 2022; Rouco et al., 2018), thus, the level of dust-Fe input

may affect N_2 fixation in the subtropical western North Pacific region via processes relating to DOP utilization. For example, during spring, when Asian dust input generally becomes the highest within the year (Zhu et al., 2007), the rates of N_2 fixation in the western North Pacific could be as high as 500–600 μmol N m^{-2} day^{-1} (Wen et al., 2022). A similar level of enhancement has also been reported in phosphate-depleted waters (<10 nM) in the tropical North Atlantic Ocean, in which dust-Fe input is approximately 10 times higher than that in the North Pacific (Luo et al., 2014; Tang et al., 2019). Therefore, the geographic pattern predicted in the prognostic biogeochemical models, in which N_2 fixation activity increases westward (Dutkiewicz et al., 2012; Monteiro et al., 2011), may be observed only when dust-Fe input is abundant. Collectively, although the results of this study are a snapshot of summer, the geographic variation in N_2 fixation with its peak in the central area possibly reflected the annually averaged pattern of N_2 fixation in the subtropical North Pacific, which is similar to that of a pattern proposed for the long-term trend of N_2 fixation based on inverse models using basin-scale phosphorus and nitrogen distributions (Wang et al., 2019).

The geographic pattern in the N_2 fixation and the distributions of the diazotrophs found in this study are also compatible with the possible effect of islands: the frequent occurrences of hotspots of diazotrophs near the islands, which were reported near the Hawaiian Islands as well as the western South Pacific (Bonnet et al., 2018; Dutheil et al., 2018; Shiozaki et al., 2014a; Sohm et al., 2010a). This phenomenon can be explained by the relatively enriched supply of either iron or phosphate from the deep layer (Itoh et al., 2021), or from the sedimentary sources around the islands (Dutheil et al., 2018), because the N_2 fixation activity near the Hawaiian Islands could be limited by either iron or phosphorus (Grabowski et al., 2008), although the activity was considered iron-limited in the eastern area in this study.

Primary production measured in the present study ranged from 11.7 to 25.1 mmol C m^{-2} day^{-1} (or 199–439 nmol C L^{-1} day^{-1}), which is consistent with those in previous reports measured by the same methods utilizing ^{13}C tracer in the subtropical North Pacific (200–300 nmol C L^{-1} day^{-1} in Gradoville et al., 2020; 19.8–21.8 mmol C m^{-2} day^{-1} in Shiozaki et al., 2017). The primary production exhibited an increasing trend with N_2 fixation in the majority of the study area (St. 1–9), potentially indicating that spatiotemporal variation in N_2 fixation controls biological production in the subtropical North Pacific. The contribution of N_2 fixation to primary productivity, however, was lower in this study (3.5–9.9%, Supporting Information Figure S5) as in previous studies (4.5–6.9 % in Shiozaki et al., 2017; ~15 % in Gradoville et al., 2020). Thus, nitrogen fixed by diazotrophs may enhance primary production by other phytoplankton through the excretion of inorganic and organic nitrogen (Glibert & Bronk, 1994; Mulholland et al., 2004), cell demise (Berman-Frank et al., 2004), and subsequent remineralization in the study area.

5 Conclusions

This study is the first field observation that shows the importance of phosphorus, as well as iron, in controlling the zonal distribution of N_2 fixation activity in the subtropical North Pacific, where phosphate concentration decreases westward but dust-Fe input from the Asian continent decreases eastward. In the western area at 180°, the N_2 fixation rates were considerably low despite the excess amount of iron relative to phosphate and correlated positively with the labile phosphoric monoesters stock, indicating that phosphorus limited the N_2 fixation activity. However, the N_2 fixation in the western area was also positively correlated with dust-Fe input, indicating likely co-limitation by phosphorus and iron. In the eastern area, with replenished phosphate and lower dust-Fe input compared to that in the western area, iron was indicated to

primarily limit N_2 fixation. The iron limitation is expected to relax around 150–170°W because there is a supply of DFe from below the euphotic zone owing to the effect of Mid-Pacific Seamounts and Hawaiian Ridge (Itoh et al. 2021) in addition to dust-Fe input from the Asian continent. The present study suggests that the zonal variation in N_2 fixation in the subtropical North Pacific is likely controlled by different processes underlying iron and phosphorus supplies. Possible phosphorus–iron co-limitation in the western area contrasts with the limitation of iron in the phosphorus-sufficient eastern area. These limitations can be relaxed by dust input as well as vertical diffusion, resulting in the observed N_2 fixation pattern in this study with a prominent peak between 150–180°W.

Acknowledgments

We would like to thank the crew members of R/V *Hakuho-maru* for their assistance in the observations and sample collection. Thanks to Mr. Y. Fujita for the collection of dissolved trace metal samples. We also thank the editors and anonymous reviewers for their careful reading and comments, which improved the manuscript greatly. This work was supported by MEXT/JSPS KAKENHI Grant Numbers JP24121005, JP24121001, JP16H04959, JP16J06708, JP16J08143, JP16K12586, JP19H05669, JP20KK0240, JP21H03592, JP24121003 and a research grant from Asahi Group Foundation.

Data Availability Statement

Data used in this article are available through UTokyo repository (http://hdl.handle.net/2261/0002005662). Spectral Radiation-Transport Model for Aerosol Species SPRINTARS is available in https://sprintars.riam.kyushu-u.ac.jp/indexe.html. We showed the range of the concentration of dissolved inorganic iron and its integrated abundance in the euphotic zone in the manuscript, which were the parameters directly used in this study, but the original data of the concentration was not shown because it is planned to be shown in another paper under preparation.

References

Adebiyi, A., Kok, J. F., Murray, B. J., Ryder, C. L., Stuut, J. B. W., Kahn, R. A., et al. (2023), A review of coarse mineral dust in the Earth system, *Aeolian Research*, *60*, doi:10.1016/j.aeolia.2022.100849

Berman-Frank, I., Bidle, K., Haramaty, L., & Falkowski, P. G. (2004), The demise of the marine cyanobacterium, *Trichodesmium* spp., via an autocatalyzed cell death pathway, *Limnology and Oceanography, 49*, 997–1005.

Berman-Frank, I., Cullen, J. T., Shaked, Y., Sherrell, R. M., & Falkowski, P. G. (2001), Iron availability, cellular iron quotas, and nitrogen fixation in *Trichodesmium*, *Limnology and Oceanography*, *46*(6), 1249–1260.

Bonnet, S., Caffin, M., Berthelot, H., Grosso, O., Benavides, M., Helias-Nunige, S., et al. (2018), In-depth characterization of diazotroph activity across the western tropical South Pacific hotspot of N_2 fixation (OUTPACE cruise), *Biogeosciences*, *15*(13), 4215–4232, doi:10.5194/bg-15-4215-2018

Böttjer, D., Dore, J. E., Karl, D. M., Letelier, R. M., Mahaffey, C., Wilson, S. T., et al. (2017), Temporal variability of nitrogen fixation and particulate nitrogen export at Station ALOHA, *Limnology and Oceanography*, *62*(1), 200–216, doi:10.1002/lno.10386

595 Browning, T. J., Achterberg, E. P., Yong, J. C., Rapp, I., Utermann, C., Engel, A., & Moore, C.
596 M. (2017), Iron limitation of microbial phosphorus acquisition in the tropical North Atlantic,
597 *Nature Communication*, *8*, 15465, doi:10.1038/ncomms15465
598 Carpenter, E. J., & Romans, K. (1991), Major Role of the Cyanobacterium Trichodesmium in
599 Nutrient Cycling in the North Atlantic Ocean, *Science*, *254*, 1356-1358
600 Cerdan-Garcia, E., Baylay, A., Polyviou, D., Woodward, E. M. S., Wrightson, L., Mahaffey, C.,
601 et al. (2022), Transcriptional responses of Trichodesmium to natural inverse gradients of Fe
602 and P availability, *ISME Journal*, *16*(4), 1055–1064, doi:10.1038/s41396-021-01151-1
603 Cheung, S., Nitanai, R., Tsurumoto, C., Endo, H., Nakaoka, S., Cheah, W., et al. (2020),
604 Physical forcing controls the basin scale occurrence of Nitrogen fixing organisms in the
605 North Pacific Ocean, *Global Biogeochemical Cycles*, *34*(9), doi:10.1029/2019gb006452
606 Christian, J. R., Lewis, M. R., & Karl, D. M. (1997), Vertical fluxes of carbon, nitrogen, and
607 phosphorus in the North Pacific Subtropical Gyre near Hawaii, *Journal of Geophysical*
608 *Research: Oceans*, *102*(C7), 15667–15677, doi:10.1029/97jc00369
609 Church, M. J., Mahaffey, C., Letelier, R. M., Lukas, R., Zehr, J. P., & Karl, D. M. (2009),
610 Physical forcing of nitrogen fixation and diazotroph community structure in the North Pacific
611 subtropical gyre, *Global Biogeochemical Cycles*, *23*(2), doi:10.1029/2008gb003418
612 Conroy, B. J., Steinberg, D. K., Song, B., Kalmbach, A., Carpenter, E. J., & Foster, R. A. (2017),
613 Mesozooplankton graze on cyanobacteria in the Amazon River Plume and Western Tropical
614 North Atlantic, *Frontiers in Microbiology*, *8*, 1436, doi:10.3389/fmicb.2017.01436
615 Dabundo, R., Lehmann, M. F., Treibergs, L., Tobias, C. R., Altabet, M. A., Moisander, P. H., &
616 Granger, J. (2014), The contamination of commercial $^{15}N_2$ gas stocks with ^{15}N-labeled nitrate
617 and ammonium and consequences for nitrogen fixation measurements, *PLoS One*, 9(10),
618 e110335, doi:10.1371/journal.pone.0110335
619 de Boyer Montégut, C., Gurvan, M., Fischer, A. S., Lazar, A., & Iudicone, D. (2004), Mixed
620 layer depth over the global ocean: An examination of profile data and a profile-based
621 climatology, *Journal of Geophysical Research*, *109*(C12), doi:10.1029/2004jc002378
622 Deutsch, C., Gruber, N., Key, R. M., Sarmiento, J. L., & Ganachaud, A. (2001), Denitrification
623 and N_2 fixation in the Pacific Ocean, *Global Biogeochemical Cycles*, *15*(2), 483–506,
624 doi:10.1029/2000gb001291
625 Deutsch, C., Sarmiento, J. L., Sigman, D. M., Gruber, N., & Dunne, J. P. (2007), Spatial
626 coupling of nitrogen inputs and losses in the ocean, *Nature*, *445*(7124), 163–167,
627 doi:10.1038/nature05392
628 Duce, R. A., & Tindale, N. W. (1991), Atmospheric transport of iron and its deposition in the
629 ocean, *Limnology and Oceanography*, *36*, 1715–1726.
630 Dugenne, M., Henderikx Freitas, F., Wilson, S. T., Karl, D. M., & White, A. E. (2020), Life and
631 death of *Crocosphaera* sp. in the Pacific Ocean: Fine scale predator-prey dynamics,
632 *Limnology and Oceanography*, *65*(11), 2603–2617, doi:10.1002/lno.11473
633 Dutheil, C., Aumont, O., Gorguès, T., Lorrain, A., Bonnet, S., Rodier, M., et al. (2018),
634 Modelling N_2 fixation related to *Trichodesmium* sp.: driving processes and impacts on
635 primary production in the tropical Pacific Ocean, *Biogeosciences*, *15*(14), 4333–4352,
636 doi:10.5194/bg-15-4333-2018
637 Dutkiewicz, S., Ward, B. A., Monteiro, F., & Follows, M. J. (2012), Interconnection of nitrogen
638 fixers and iron in the Pacific Ocean: Theory and numerical simulations, *Global*
639 *Biogeochemical Cycles*, *26*(1), GB1012, doi:10.1029/2011gb004039
640 Falkowski, P. G., Barber, B. T., & Smeacek, V. (1998), Biogeochemical Controls and Feedbacks

on Ocean Primary Production, *Science*, *281*(5374), 200–206.
Galloway, J. N., Dentener, F. J., Capone, D. G., Boyer, E. W., Howarth, R. W., Seitzinger, S. P., et al. (2004), Nitrogen Cycles: Past, Present and Future, *Biogeochemistry*, *70*, 153–226, https://doi.org/10.1007/s10533-004-0370-0
Garcia, N. S., Fu, F., Sedwick, P. N., & Hutchins, D. A. (2015), Iron deficiency increases growth and nitrogen-fixation rates of phosphorus-deficient marine cyanobacteria, *The ISME Journal, 9*(1), 238–245, doi:10.1038/ismej.2014.104
Glibert, P. M. & Bronk, D. A. (1994), Release of dissolved organic nitrogen by marine diazotrophic cyanobacteria, *Trichodesmium* spp., *Applied and Environmental Microbiology*, *60*, 3996–4000, doi:10.1128/aem.60.11.3996-4000.1994
Grabowski, M. N. W., Church, M. J., & Karl, D. M. (2008), Nitrogen fixation rates and controls at Stn ALOHA, *Aquatic Microbial Ecology*, *52*, 175–183, doi:10.3354/ame01209
Gradoville, M. R., Farnelid, H., White, A. E., Turk−Kubo, K. A., Stewart, B., Ribalet, F., et al. (2020), Latitudinal constraints on the abundance and activity of the cyanobacterium UCYN - A and other marine diazotrophs in the North Pacific, *Limnology and Oceanography, 65*(8), 1858–1875, doi:10.1002/lno.11423
Gruber, N., & Sarmiento, J. L. (1997), Global patterns of marine nitrogen fixation and denitrification, *Global Biogeochemical Cycles*, *11*(2), 235–266, doi:10.1029/97gb00077.
Hama, T., Miyazaki, T., Ogawa, Y., Iwakuma, T., Takahashi, M., Otsuki, A., & Ichimura, S. (1983), Measurement of photosynthetic production of a marine phytoplankton population using a stable ^{13}C isotope, *Marine Biology*, *73*, 31–36.
Hashihama, F., Furuya, K., Kitajima, S., Takeda, S., Takemura, T., & Kanda, J. (2009), Macro-scale exhaustion of surface phosphate by dinitrogen fixation in the western North Pacific, *Geophysical Research Letters*, *36*(3), doi:10.1029/2008gl036866
Hashihama, F., Saito, H., Shiozaki, T., Ehama, M., Suwa, S., Sugiyama, T., et al. (2020), Biogeochemical controls of particulate phosphorus distribution across the oligotrophic subtropical Pacific Ocean, *Global Biogeochemical Cycles*, *34*(9), doi:10.1029/2020gb006669
Itoh, S., Kaneko, H., Kouketsu, S., Okunishi, T., Tsutsumi, E., Ogawa, H., & Yasuda, I. (2021), Vertical eddy diffusivity in the subsurface pycnocline across the Pacific, *Journal of Oceanography*, *77*(2), 185–197, doi:10.1007/s10872-020-00589-9
Karl, D., Michaels, A., Bergman, B., Capone, D., Carpenter, E., Letelier, R., et al. (2002), Dinitrogen fixation in the world's oceans, *Biogeochemistry*, *57/58*, 47–98.
Letelier, R. M., Bjorkman, K. M., Church, M. J., Hamilton, D. S., Mahowald, N. M., Scanza, R. A., et al. (2019), Climate-driven oscillation of phosphorus and iron limitation in the North Pacific Subtropical Gyre, *Proceedings of the National Academy of Sciences of the United States of America*, *116*(26), 12720–12728, doi:10.1073/pnas.1900789116
Liang, Z., Letscher, R. T., & Knapp, A. N. (2022), Dissolved organic phosphorus concentrations in the surface ocean controlled by both phosphate and iron stress, *Nature Geoscience*, *15*(8), 651–657, doi:10.1038/s41561-022-00988-1
Luo, C., Mahowald, N., Bond, T., Chuang, P. Y., Artaxo, P., Siefert, R., et al. (2008), Combustion iron distribution and deposition, *Global Biogeochemical Cycles*, *22*(1), doi:10.1029/2007gb002964
Luo, Y. W., Lima, I. D., Karl, D. M., Deutsch, C. A., & Doney, S. C. (2014), Data-based assessment of environmental controls on global marine nitrogen fixation, *Biogeosciences*, *11*(3), 691–708, doi:10.5194/bg-11-691-2014
Mahaffey, C., Reynolds, S., Davis, C. E., & Lohan, M. C. (2014), Alkaline phosphatase activity

687 in the subtropical ocean: insights from nutrient, dust and trace metal addition experiments,
688 *Frontiers in Marine Science*, *1*, doi:10.3389/fmars.2014.00073
689 Martiny, A. C., Lomas, M. W., Fu, W., Boyd, P. W., Chen, Y. I. L., Cutter, G. A., et al. (2019),
690 Biogeochemical controls of surface ocean phosphate, *Science Advances*, *5*(8), eaax0341, doi:
691 10.1126/sciadv.aax0341
692 Mohr, W., Grosskopf, T., Wallace, D. W., & LaRoche, J. (2010), Methodological
693 underestimation of oceanic nitrogen fixation rates, *PLoS One*, *5*(9), e12583,
694 doi:10.1371/journal.pone.0012583
695 Monteiro, F. M., Dutkiewicz, S., & Follows, M. J. (2011), Biogeographical controls on the
696 marine nitrogen fixers, *Global Biogeochemical Cycles*, *25*(2), doi:10.1029/2010gb003902
697 Montoya, J. P., Holl, C. M., Zehr, J. P., Hansen, A., Villareal, T. A., & Capone, D. G. (2004),
698 High rates of N_2 fixation by unicellular diazotrophs in the oligotrophic Pacific Ocean, *Nature*,
699 *430*(7003), 1027–1031, doi:10.1038/nature02824
700 Montoya, J. P., Voss, M., Kahler, P., & Capone, D. G. (1996), A simple, high-precision, high-
701 sensitivity tracer assay for N_2 fixation, *Applied and Environmental Microbiology*, *62*(3), 986–
702 993.
703 Moore, M. C., Mills, M. M., Achterberg, E. P., Geider, R. J., LaRoche, J., Lucas, M. I., et al.
704 (2009), Large-scale distribution of Atlantic nitrogen fixation controlled by iron availability,
705 *Nature Geoscience*, *2*(12), 867–871, doi:10.1038/ngeo667
706 Mulholland, M. R., Bronk, D.A., & Capone, D. G. (2004), Dinitrogen fixation and release of
707 ammonium and dissolved organic nitrogen by *Trichodesmium* IMS101, *Aquatic Microbial*
708 *Ecology, 37*, 85-94.
709 Nishioka, J., & Obata, H. (2017), Dissolved iron distribution in the western and central subarctic
710 Pacific: HNLC water formation and biogeochemical processes, *Limnology and Oceanography*,
711 *62*(5), 2004–2022, doi:10.1002/lno.10548
712 Obata, H., & van den Berg, C. M. G. (2001), Determination of picomolar levels of iron in
713 seawater using catalytic cathodic stripping voltammetry, *Analytical Chemistry*, *73*(11), 2522–
714 2528, doi:10.1021/ac001495d
715 Rijkenberg, M. J. A., Slagter, H. A., Rutgers van der Loeff, M., van Ooijen, J. & Gerringa, L. J.
716 A. (2018) Dissolved Fe in the deep and upper Arctic Ocean with a focus on Fe limitation in
717 the Nansen Basin. *Frontiers in Marine Scienc*e, 5(88). doi: 10.3389/fmars.2018.00088
718 Rouco, M., Frischkorn, K. R., Haley, S. T., Alexander, H., & Dyhrman, S. T. (2018),
719 Transcriptional patterns identify resource controls on the diazotroph *Trichodesmium* in the
720 Atlantic and Pacific oceans, *ISME J*, *12*(6), 1486–1495, doi:10.1038/s41396-018-0087-z
721 Saito, M. A., Goepfert, T. J., & Ritt, J. T. (2008), Some thoughts on the concept of colimitation:
722 Three definitions and the importance of bioavailability, *Limnology and Oceanography, 53*(1),
723 276–290, doi:10.4319/lo.2008.53.1.0276
724 Sato, R., & Suzuki, Y. (2010), Carbon and Nitrogen stable isotope analysis by EA/IRMS,
725 *Researches in Organic Geochemistry*, *26*, 21–29, https://doi.org/10.20612/rog.26.0_21
726 Shiozaki, T., Bombar, D., Riemann, L., Hashihama, F., Takeda, S., Yamaguchi, T., et al. (2017),
727 Basin scale variability of active diazotrophs and nitrogen fixation in the North Pacific, from
728 the tropics to the subarctic Bering Sea, *Global Biogeochemical Cycles*, *31*(6), 996–1009,
729 doi:10.1002/2017gb005681
730 Shiozaki, T., Furuya, K., Kodama, T., Kitajima, S., Takeda, S., Takemura, T., & Kanda, J.
731 (2010), New estimation of N_2 fixation in the western and central Pacific Ocean and its
732 marginal seas, *Global Biogeochemical Cycles*, *24*(1), doi:10.1029/2009gb003620

Shiozaki, T., Furuya, K., Kodama, T., & Takeda, S. (2009), Contribution of N_2 fixation to new production in the western North Pacific Ocean along 155°E, *Marine Ecology Progress Series*, *377*, 19–32, doi:10.3354/meps07837

Shiozaki, T., Kodama, T., & Furuya, K. (2014a), Large-scale impact of the island mass effect through nitrogen fixation in the western South Pacific Ocean, *Geophysical Research Letters*, *41*(8), 2907–2913, doi:10.1002/2014gl059835

Shiozaki, T., Takeda, S., Itoh, S., Kodama, T., Liu, X., Hashihama, F., & Furuya, K. (2015), Why is *Trichodesmium* abundant in the Kuroshio?, *Biogeosciences*, *12*(23), 6931–6943, doi:10.5194/bg-12-6931-2015

Sohm, J. A., Subramaniam, A. G., T. E. Carpenter, E. J., & Capone, D. G. (2011a), Nitrogen fixation by *Trichodesmium* spp. and unicellular diazotrophs in the North Pacific Subtropical Gyre, *Journal of Geophysical Research*, *116*(G03002), doi:10.1029/2010JG001513

Sohm, J. A., Webb, E. A., & Capone, D. G. (2011b), Emerging patterns of marine nitrogen fixation, *Nature Reviews Microbiology*, *9*(7), 499–508, doi:10.1038/nrmicro2594

Suzuki, R., & Ishimaru, T. (1990), An improved method for the determination of phytoplankton chlorophyll using N, N-dimethylformamide, *Journal of the Oceanographical Society of Japan*, *46*, 190–194.

Takemura, T. (2005), Simulation of climate response to aerosol direct and indirect effects with aerosol transport-radiation model, *Journal of Geophysical Research*, *110*(D2), doi:10.1029/2004jd005029

Takemura, T., Okamoto, H., Maruyama, Y., Numaguti, A., Higurashi, A., & Nakajima, T. (2000), Global three-dimensional simulation of aerosol optical thickness distribution of various origins, *Journal of Geophysical Research: Atmospheres*, *105*(D14), 17853–17873, doi:10.1029/2000jd900265

Takemura, T., Uno, I., Nakajima, T., Higurashi, A., & Sano, I. (2002), Modeling study of long-range transport of Asian dust and anthropogenic aerosols from East Asia, *Geophysical Research Letters*, *29*(24), 2158, doi:10.1029/2002gl016251

Tang, W., & Cassar, N. (2019), Data-driven modeling of the distribution of diazotrophs in the global ocean, *Geophysical Research Letters*, 12258–12269, doi:10.1029/2019GL084376

Tang, W., Wang, S., Fonseca-Batista, D., Dehairs, F., Gifford, S., Gonzalez, A. G., et al. (2019), Revisiting the distribution of oceanic N_2 fixation and estimating diazotrophic contribution to marine production, *Nature Communication*, *10*(1), 831, doi:10.1038/s41467-019-08640-0

Tanita, I., Shiozaki, T., Kodama, T., Hashihama, F., Sato, M., Takahashi, K., & Furuya, K. (2021), Regionally variable responses of nitrogen fixation to iron and phosphorus enrichment in the Pacific Ocean, *Journal of Geophysical Research: Biogeosciences*, *126*(9), doi:10.1029/2021jg006542

Wang, H., & Luo, Y.-W. (2022), Top-down control on major groups of global marine diazotrophs, *Acta Oceanologica Sinica*, *41*(8), 111-119, doi:10.1007/s13131-021-1956-2

Wang, W. L., Moore, J. K., Martiny, A. C., & Primeau, F. W. (2019), Convergent estimates of marine nitrogen fixation, *Nature*, *566*(7743), 205–211, doi:10.1038/s41586-019-0911-2

Ward, B. A., Dutkiewicz, S., Moore, C. M., & Follows, M. J. (2013), Iron, phosphorus, and nitrogen supply ratios define the biogeography of nitrogen fixation, *Limnology and Oceanography*, *58*(6), 2059–2075, doi:10.4319/lo.2013.58.6.2059

Watkins-Brandt, K. S., Letelier, R. M., Spitz, Y. H., Church, M. J., Böttjer, D., & White, A. E. (2011), Addition of inorganic or organic phosphorus enhances nitrogen and carbon fixation in the -oligotrophic North Pacific, *Marine Ecology Progress Series*, *432*, 17–29,

doi:10.3354/meps09147
Weiss, R. F. (1970), The solubility of nitrogen, oxygen, and argon in water and seawater. *Deep-Sea Research*, 29, 459–469.
Welschmeyer, N. A. (1994), Fluorometric analysis of chlorophyll *a* in the presence of chlorophyll *b* and phopigments, *Limnology and Oceanography*, *39*(8), 1985–1992.
Wen, Z., Browning, T. J., Cai, Y., Dai, R., Zhang, R., Du, C., et al. (2022), Nutrient regulation of biological nitrogen fixation across the tropical western North Pacific, *Science Advances*, *8*(5), eabl7564, doi:10.1126/sciadv.abl7564
White, A. E., Granger, J., Selden, C., Gradoville, M. R., Potts, L., Bourbonnais, A., et al. (2020), A critical review of the $^{15}N_2$ tracer method to measure diazotrophic production in pelagic ecosystems, *Limnology and Oceanography: Methods*, *18*(4), 129–147, doi:10.1002/lom3.10353
Wilson, C., Villareal, T. A., Maximenko, N., Bograd, S. J., Montoya, J. P., & Schoenbaechler, C. A. (2008), Biological and physical forcings of late summer chlorophyll blooms at 30°N in the oligotrophic Pacific, *Journal of Marine Systems*, *69*(3–4), 164–176, doi:10.1016/j.jmarsys.2005.09.018
Yamaguchi, T., Sato, M., Hashihama, F., Ehama, M., Shiozaki, T., Takahashi, K., & Furuya, K. (2019), Basin−scale variations in labile dissolved phosphoric monoesters and diesters in the central North Pacific Ocean, *Journal of Geophysical Research: Oceans*, *124*(5), 3058–3072, doi:10.1029/2018jc014763
Yamaguchi, T., Sato, M., Hashihama, F., Kato, H., Sugiyama, T., Ogawa, H., et al. (2020), Longitudinal and vertical variations of dissolved labile phosphoric mnoesters and desters in the subtropical North Pacific, *Frontiers in Microbiology*, *11*, 570081, doi:10.3389/fmicb.2020.570081
Young, C. L., & Ingall, E. D. (2010). Marine dissolved organic phosphorus composition: insights from samples recovered using combined electrodialysis/reverse osmosis. *Aquatic Geochemistry, 16*, 563–574, doi:10.1007/s10498-009-9087-y
Zhu, A., Ramanathan, V., Li, F., & Kim, D. (2007), Dust plumes over the Pacific, Indian, and Atlantic oceans: Climatology and radiative impact, *Journal of Geophysical Research*, *112*(D16), doi:10.1029/2007jd008427

References from Supporting Information

Foster, R. A., Subramaniam, A., Mahaffey, C., Carpenter, E. J., Capone, D. G., & Zehr, J. P. (2007), Influence of the Amazon River plume on distributions of free-living and symbiotic cyanobacteria in the western tropical north Atlantic Ocean, *Limnology and Oceanography*, 52(2), 517–532, doi:10.4319/lo.2007.52.2.0517
Moisander, P. H., Beinart, R. A., Hewson, I., White, A. E., Johnson, K. S., Carlson, C. A., et al. (2010), Unicellular cyanobacterial distributions broaden the oceanic N_2 fixation domain, *Science*, *327*(5972), 1512–1514, doi:10.1126/science.1185468
Shiozaki, T., Chen, Y. l. L., Lin, Y. H., Taniuchi, Y., Sheu, D. S., Furuya, K., & Chen, H. Y. (2014b), Seasonal variations of unicellular diazotroph groups A and B, and *Trichodesmium* in the northern South China sea and neighboring upstream Kuroshio current, *Continental Shelf Research*, *80*, 20–31, doi:10.1016/j.csr.2014.02.015
Shiozaki, T., Ijichi, M., Kodama, T., Takeda, S., & Furuya, K. (2014c), Heterotrophic bacteria as major nitrogen fixers in the euphotic zone of the Indian Ocean, *Global Biogeochemical Cycles*, *28*(10), 1096–1110, doi:10.1002/2014gb004886

824 **Figure Legends**

825 **Figure 1.** Stations where samplings and observations were performed from 21 August to 1
826 October, 2017 during the KH-17-4 cruise. Chlorophyll *a* concentration derived from MODIS-
827 Aqua (https://oceancolor.gsfc.nasa.gov/l3/) in September 2017 is also shown.
828
829 **Figure 2.** Profiles of the environmental variables at the stations along the cruise track during the
830 KH-17-4 cruise. Vertical profiles of (a) temperature, (b) salinity, concentrations of (c)
831 chlorophyll *a*, (d) nitrate, (e) phosphate, (f) labile phosphoric monoesters, (g) N_2 fixation activity
832 and (h) primary production. Black bold line indicates the 1% light depth. White dashed line
833 indicates mixed layer depth. The sampling point with black cross in (g) indicates the layer where
834 the rate of N_2 fixation was below the detection limit.
835
836 **Figure 3.** Zonal variations in phosphorus and iron conditions and N_2 fixation activity along the
837 cruise track during the KH-17-4. (a) The calculated daily flux of iron deposition as atmospheric
838 dust (dust-Fe), which was modeled using SPRINTARS for 14 days before the observation, and
839 the integrated amounts of dissolved inorganic iron (DFe) in the euphotic zone. Error bars for
840 dust-Fe indicate the standard deviations for the daily averaged values. Crosses and solid lines in
841 the box plot indicate the averages and medians, respectively. (b) The integrated amounts of
842 phosphate and labile phosphoric monoesters in the euphotic zone. (c) The integrated rates of N_2
843 fixation activity in the water column. Error bars indicate the standard deviations.
844
845 **Figure 4.** Relationships between N_2 fixation activity in the water column and the environmental
846 variables during the KH-17-4 cruise. The relationship with (a) the calculated 14-days average of
847 the daily flux of iron deposition as atmospheric dust (dust-Fe) before the observation, which was
848 modeled using SPRINTARS, and the integrated amount in the euphotic zone of (b) dissolved
849 inorganic iron (DFe), (c) phosphate, and (d) labile phosphoric monoesters. Station numbers are
850 shown beside the plots. Regression lines are shown when the relationships were significant (p
851 <0.05). Regression analyses were performed separately for the eastern and western parts of the
852 transect.
853
854 **Figure 5.** Zonal variations in iron and phosphate fluxes and their relative decoupling magnitudes
855 during the KH-17-4 cruise. (a) Soluble dust-Fe flux and vertical DFe diffusion flux into the
856 euphotic zone and their proportions in the total Fe flux. (b) Vertical phosphate diffusion flux into
857 the euphotic zone. (c) The magnitude of excess iron supply relative to phosphate (total Fe* flux)
858 and excess DFe amount relative to phosphate in the euphotic zone (euphotic-zone DFe*). DFe =
859 dissolved inorganic iron. Dust-Fe = modeled 14-days average of the daily flux of iron deposition
860 as atmospheric dust before the observation. Soluble dust-Fe flux was calculated from dust-Fe,
861 considering 0.45% solubility (Luo et al., 2008). Vertical diffusion fluxes of DFe and phosphate
862 were calculated from the vertical gradient of DFe and phosphate using the eddy diffusivities
863 observed during the same cruise in the subsurface pycnocline (Itoh et al., 2021). Total Fe flux =
864 soluble dust-Fe flux + vertical DFe diffusion flux. Total Fe* flux = Total Fe flux − vertical
865 phosphate diffusion flux × 0.48/1000. Euphotic-zone DFe* = DFe amount in the euphotic zone −
866 phosphate amount in the euphotic zone × 0.48/1000. Negative values were considered zero for
867 calculating the proportions in (a).
868

869 **Figure 6.** Relationships between N_2 fixation activity in the water column and relative decoupling
870 magnitudes between iron and phosphorus supply or abundance during the KH-17-4 cruise; (a)
871 the magnitude of excess iron supply relative to phosphate (total Fe* flux) and (b) depth-
872 integrated excess DFe amount relative to phosphate in the euphotic zone (euphotic zone DFe*).
873 Station numbers are shown alongside the plots. Regression lines are shown when the
874 relationships are significant (p <0.05). Regression analyses were performed separately for the
875 eastern and western areas of the transect. DFe = dissolved inorganic iron. Total Fe* flux =
876 soluble dust-Fe flux + vertical DFe diffusion flux − vertical phosphate diffusion flux × 0.48/1000.
877 Euphotic-zone DFe* = DFe amount in the euphotic zone − phosphate amount in the euphotic
878 zone × 0.48/1000.
879
880 **Figure 7.** Zonal variations in depth-integrated abundances of *nifH* gene for the diazotrophs
881 quantified by qPCR analyses and N_2 fixation activity during the KH-17-4 cruise.

Figures.

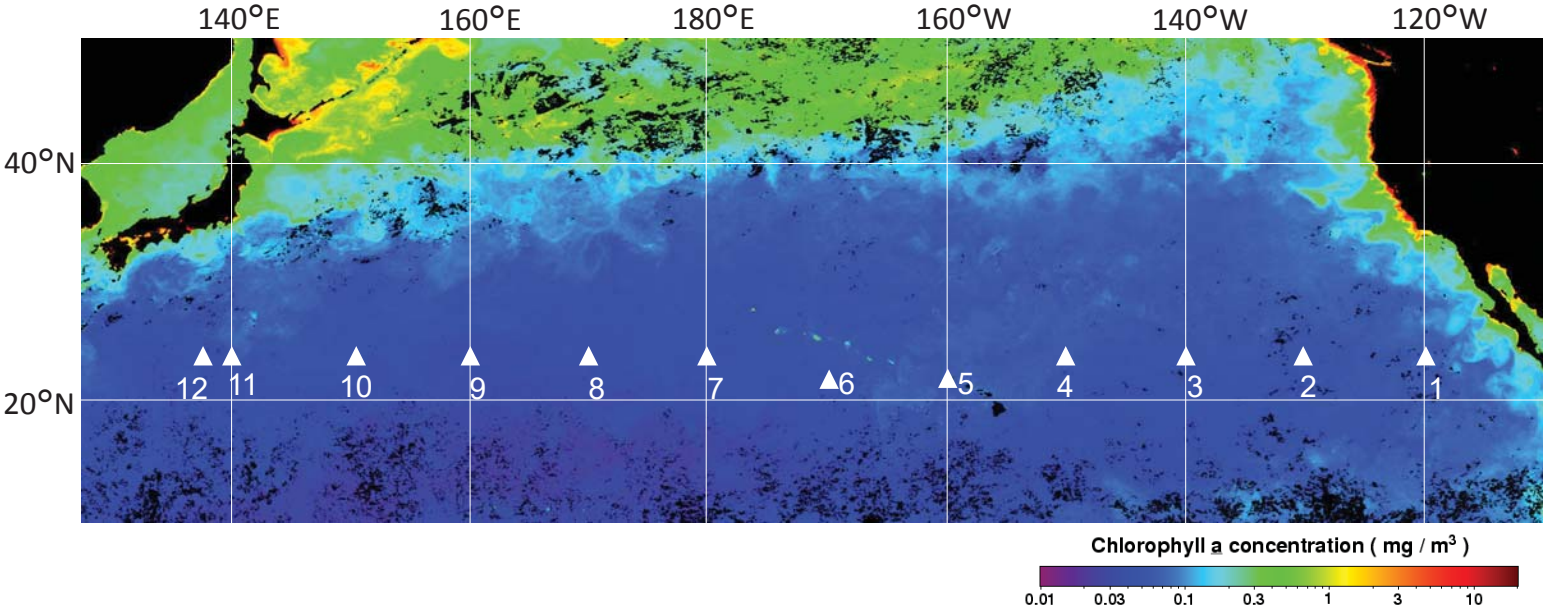
140°E
160°E
180°E
160°W
140°W
120°W
40°N
20°N
12
11
10
9
8
7
6
5
4
3
2
1
Chlorophyll a concentration (mg / m3)
0.01
0.03
0.1
0.3
1
3
10

(a) Temperature (°C)

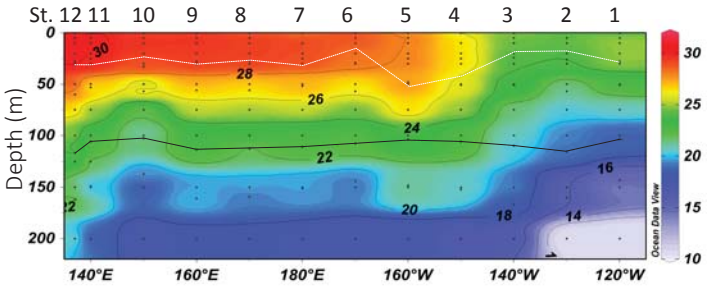

(b) Salinity

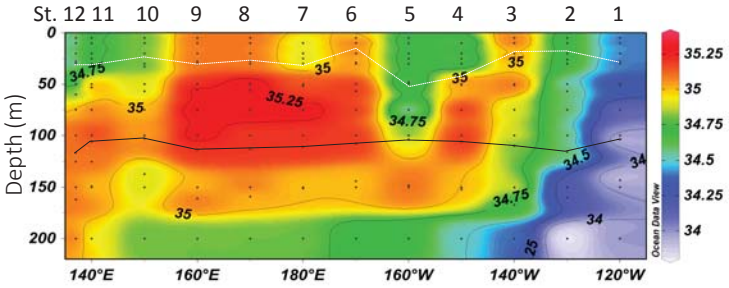

(c) Chlorophyll *a* (µg/L)

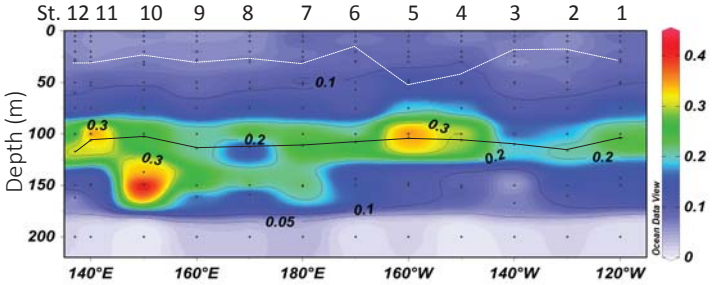

(d) Nitrate (nM)

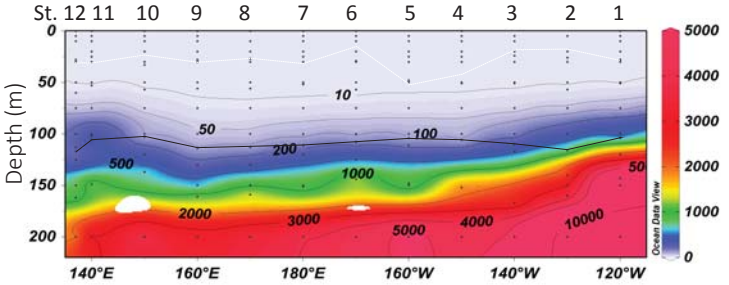

(e) Phosphate (nM)

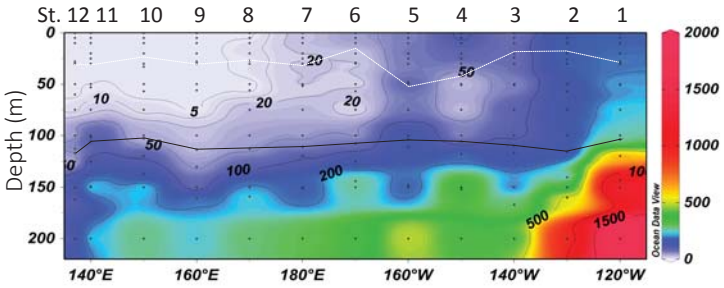

(f) Phosphoric monoesters (nM)

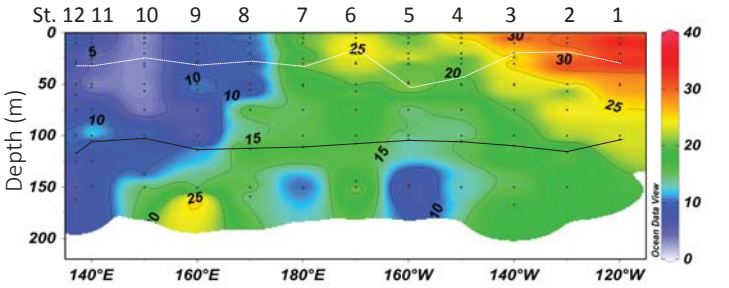

(g) N_2 fixation activity (nmol N L^{-1} day^{-1})

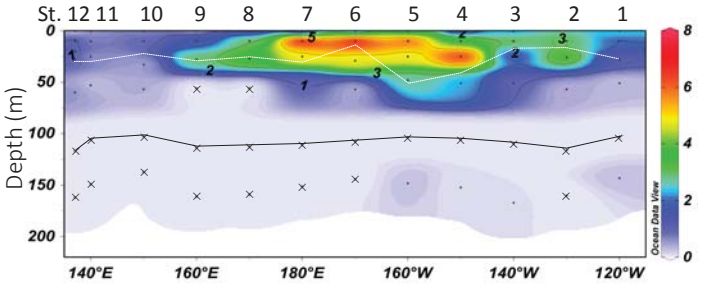

(h) Primary production (nmol C L^{-1} day^{-1})

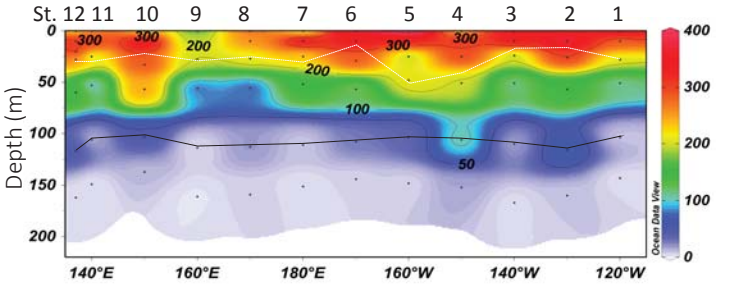

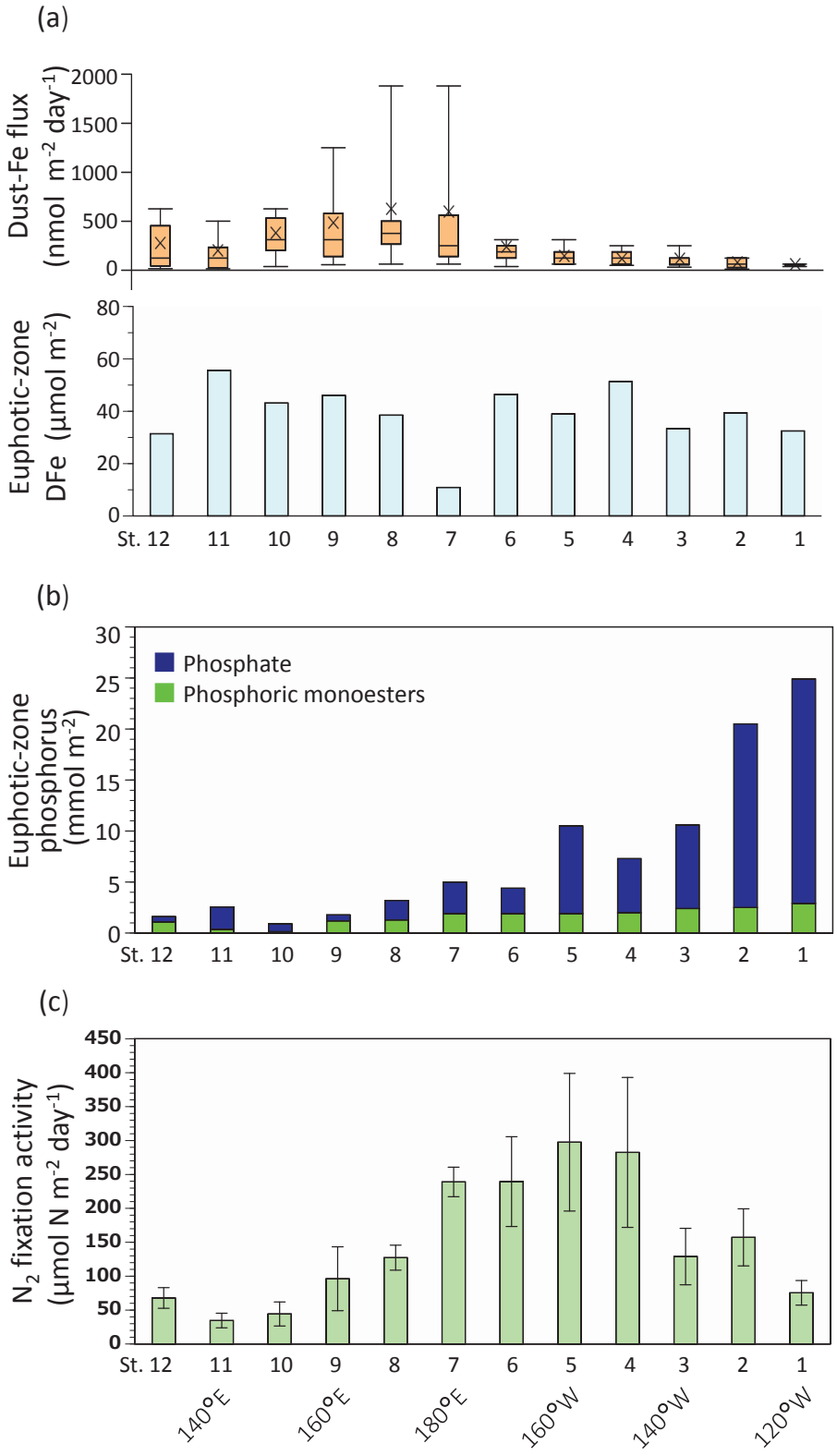
(a)
Dust-Fe flux (nmol m-2 day-1)
2000
1500
1000
500
0
Euphotic-zone DFe (µmol m-2)
80
60
40
20
0
St. 12 11 10 9 8 7 6 5 4 3 2 1
(b)
Euphotic-zone phosphorus (mmol m-2)
Phosphate
Phosphoric monoesters
30
25
20
15
10
5
0
St. 12 11 10 9 8 7 6 5 4 3 2 1
(c)
N2 fixation activity (µmol N m-2 day-1)
450
400
350
300
250
200
150
100
50
0
St. 12 11 10 9 8 7 6 5 4 3 2 1
140°E
160°E
180°E
160°W
140°W
120°W

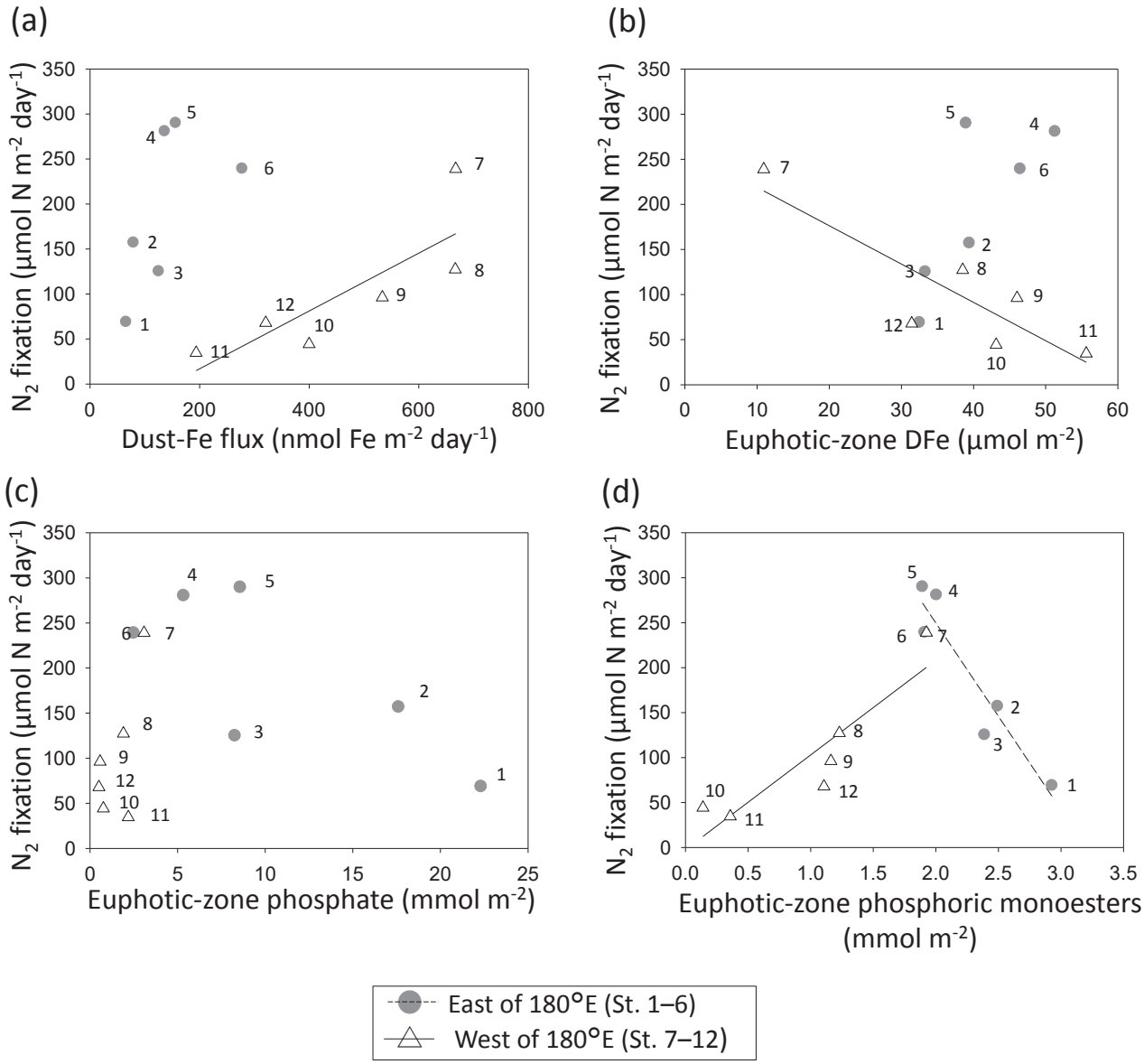
(a)
N2 fixation (µmol N m-2 day-1)
Dust-Fe flux (nmol Fe m-2 day-1)
(b)
N2 fixation (µmol N m-2 day-1)
Euphotic-zone DFe (µmol m-2)
(c)
N2 fixation (µmol N m-2 day-1)
Euphotic-zone phosphate (mmol m-2)
(d)
N2 fixation (µmol N m-2 day-1)
Euphotic-zone phosphoric monoesters (mmol m-2)
East of 180°E (St. 1–6)
West of 180°E (St. 7–12)

(a) Iron flux

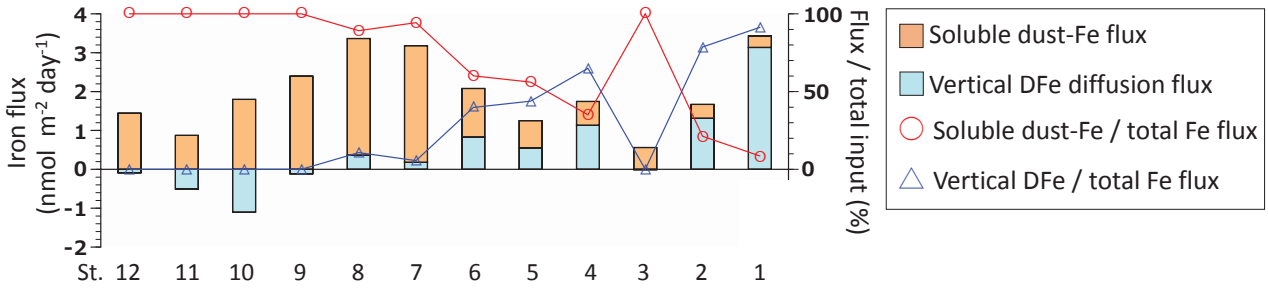

(b) Vertical phosphate diffusion flux

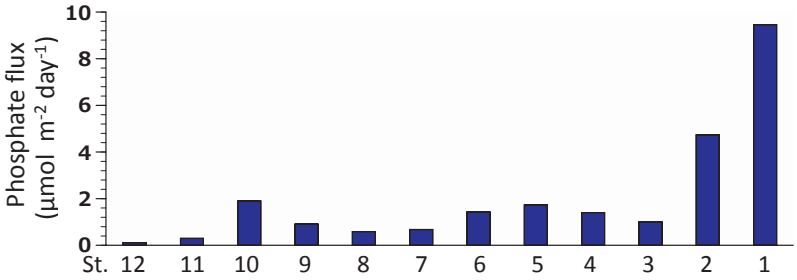

(c) Total Fe* flux and euphotic-zone DFe*

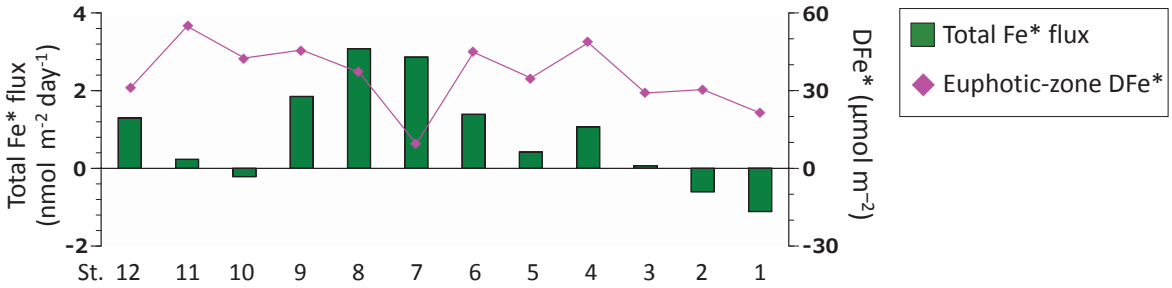

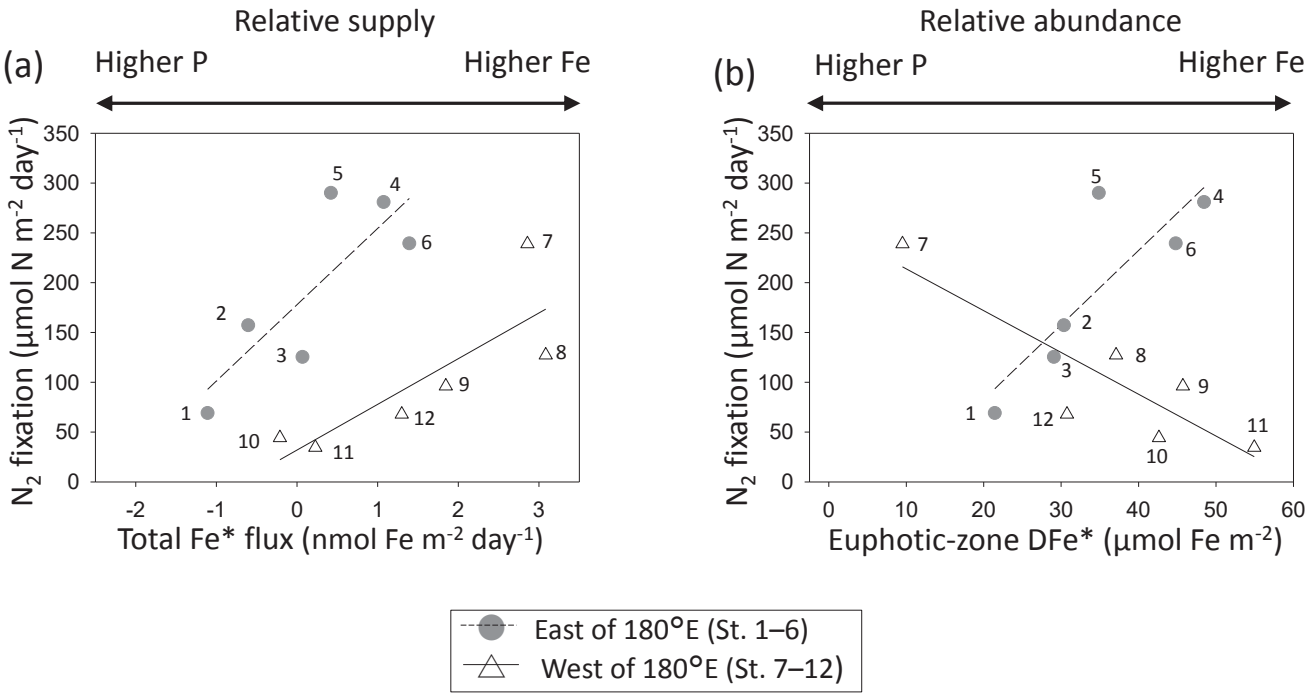
(a)
Relative supply
Higher P
Higher Fe
N_2 fixation (µmol N m^{-2} day^{-1})
Total Fe* flux (nmol Fe m^{-2} day^{-1})
(b)
Relative abundance
Higher P
Higher Fe
N_2 fixation (µmol N m^{-2} day^{-1})
Euphotic-zone DFe* (µmol Fe m^{-2})
East of 180°E (St. 1–6)
West of 180°E (St. 7–12)

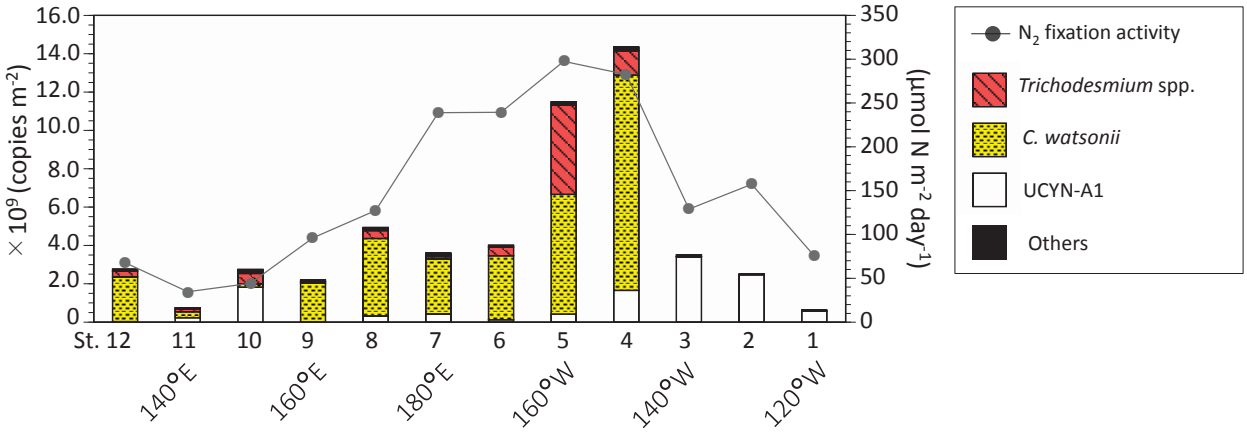
16.0
14.0
12.0
10.0
8.0
6.0
4.0
2.0
0
× 10⁹ (copies m⁻²)
350
300
250
200
150
100
50
0
(μmol N m⁻² day⁻¹)
St. 12
11
10
9
8
7
6
5
4
3
2
1
140°E
160°E
180°E
160°W
140°W
120°W
N2 fixation activity
Trichodesmium spp.
C. watsonii
UCYN-A1
Others